

Atomic quantum gases in periodically driven optical lattices

André Eckardt*

Max-Planck-Institut für Physik komplexer Systeme,
Nöthnitzer Str. 38, 01187 Dresden, Germany

(Dated: June 26, 2016)

Time periodic forcing in the form of coherent radiation is a standard tool for the coherent manipulation of small quantum systems like single atoms. In the last years, periodic driving has more and more also been considered as a means for the coherent control of many-body systems. In particular, experiments with ultracold quantum gases in optical lattices subjected to periodic driving in the lower kilohertz regime have attracted a lot of attention. Milestones include the observation of dynamic localization, the dynamic control of the quantum phase transition between a bosonic superfluid and a Mott insulator, as well as the dynamic creation of strong artificial magnetic fields and topological band structures. This article reviews these recent experiments and their theoretical description. Moreover, fundamental properties of periodically driven many-body systems are discussed within the framework of Floquet theory, including heating, relaxation dynamics, anomalous topological edge states, and the response to slow parameter variations.

CONTENTS

I. Introduction	1
II. Some general properties of Floquet systems	3
III. Quantum-gas experiments and their basic description	6
A. Neutral atoms in optical lattices	6
B. Dynamic localization	7
C. “Photon”-assisted coherent tunneling	9
D. Dynamic control of the bosonic superfluid-to-Mott-insulator transition	11
E. Kinetic frustration	12
F. Artificial magnetic fields – High-frequency schemes	14
1. Moving-secondary-lattice scheme	16
2. Asymmetric-lattice-shaking scheme	17
3. Further possibilities	18
G. Coherent resonant band coupling	18
H. Floquet topological insulators	19
I. Floquet engineering of interactions	20
IV. The Floquet picture	21
A. Extended Floquet Hilbert space	22
B. High-frequency approximation	22
C. Heating and long-time limit	23
D. Anomalous topological edge states	25
E. Two-time formalism	27
F. Adiabatic state preparation	27
V. Conclusion and outlook	28
Acknowledgments	28
References	28

I. INTRODUCTION

While time-periodic forcing in the form of coherent radiation is a standard tool for the coherent manipulation

of small quantum systems like single atoms, traditionally it plays much less of a role in the context of many-body systems. However, recent experiments with ultracold atomic quantum gases in optical lattices demonstrate that periodic forcing can also be a powerful tool for the coherent manipulation of *many-body* states and their dynamics. These experiments include the control of ballistic expansion of Bose-Einstein condensates via periodic driving (Lignier *et al.*, 2007), coherent resonant AC-induced tunneling (Alberti *et al.*, 2009; Haller *et al.*, 2010; Ivanov *et al.*, 2008; Sias *et al.*, 2008), the dynamic control of the quantum phase transition between a bosonic Mott insulator and a superfluid (Zenesini *et al.*, 2009), the creation of kinetic frustration (Struck *et al.*, 2011), artificial magnetic fields (Aidelsburger *et al.*, 2013, 2011; Atala *et al.*, 2014; Kennedy *et al.*, 2015; Miyake *et al.*, 2013; Struck *et al.*, 2012, 2013) and topological band structures (Aidelsburger *et al.*, 2015; Jotzu *et al.*, 2014), coherent band coupling (Bakr *et al.*, 2011; Gemelke *et al.*, 2005; Ha *et al.*, 2015; Parker *et al.*, 2013), as well the coherent control of interaction blockade by means of resonant forcing (Bakr *et al.*, 2011; Ma *et al.*, 2011; Meinert *et al.*, 2016). It is the fact that ultracold quantum gases are extremely clean, very well isolated from their environment, and highly controllable in a time-dependent fashion that allowed for these recent advances.

On a theoretical level, the idea of controlling lattice systems by means of strong periodic forcing (beyond the regime of linear response) dates back to the work of Dunlap and Kenkre, 1986. They investigated the spreading of a localized particle in a tight-binding chain under the influence of a sinusoidal force $F_\omega \cos(\omega t)$. The forcing was found to slow down the linear spreading of the wave function by a factor of $\mathcal{J}_0(dF_\omega/\hbar\omega)$, with lattice constant d and \mathcal{J}_m denoting the Bessel function of the first kind of order m . The possibility to tune this factor to zero,

* eckardt@pks.mpg.de

and thus completely suppress the dispersion of the wave packet, was termed *dynamic localization*. The effect was much later observed with a Bose-Einstein condensate in a shaken optical lattice (Creffield *et al.*, 2010; Eckardt *et al.*, 2009; Lignier *et al.*, 2007) and in arrays of optical wave guides, where one spatial direction plays the role of time (Dreisow *et al.*, 2008; Iyer *et al.*, 2007; Lenz *et al.*, 2003; Longhi *et al.*, 2006; Szameit *et al.*, 2009, 2010). It can be understood in terms of an effective modification of the band width (or the tunneling matrix element) by the same factor (Holthaus, 1992). Whereas this modification is exact in the infinite translational invariant chain, for large frequencies it still holds approximately if the translational symmetry is broken.¹ This effect was used in a series of proposals for the AC control of quantum mechanical localization by effectively squeezing the tunneling parameter relative to the strength of an isolated defect (Hone and Holthaus, 1993), on-site disorder (Holthaus *et al.*, 1995), or a quasiperiodic perturbation (Drese and Holthaus, 1997a). The last reference is also the first proposal for the application of such a coherent control scheme to a system of ultracold atoms in a driven optical lattice. More recently, it was argued that for large driving frequencies the effective modification of the tunneling remains approximately valid also in the presence of interactions, so that it should be possible to control also the interaction-driven localization transition from a bosonic superfluid to a Mott-insulating state (Eckardt *et al.*, 2005), an effect later observed experimentally (Zenesini *et al.*, 2009).

An important concept for the coherent control of time-periodically driven quantum systems, also called *Floquet systems*, is the *Floquet Hamiltonian* $\hat{H}_{t_0}^F$. It is defined to reproduce the time evolution generated by the Hamiltonian $\hat{H}(t) = \hat{H}(t + T)$ over one driving cycle T ,²

$$\hat{U}(t_0 + T, t_0) \equiv \exp\left(-\frac{i}{\hbar} T \hat{H}_{t_0}^F\right). \quad (1)$$

Here $\hat{U}(t_2, t_1)$ denotes the time evolution operator from time t_1 to time t_2 . Thus, when looking at the time evolution in a stroboscopic fashion in steps of the driving

period T , the system behaves effectively as if it was described by the *time-independent* Hamiltonian $\hat{H}_{t_0}^F$. The effect of dynamic localization has to be understood in this sense.

The simple equation (1) suggests a general strategy for the controlled manipulation of quantum systems. By tailoring the Hamiltonian $\hat{H}(t)$ of a system and its periodic time dependence the physics of a Floquet Hamiltonian $\hat{H}_{t_0}^F$ with desired properties can be realized. This concept of *Floquet engineering* becomes of practical relevance, provided three conditions are fulfilled:

- (i) The system allows for the implementation of a suitable time-periodic driving scheme.
- (ii) The system is well isolated from its environment such that dissipative processes happen on a time scale much longer than the driving period T .
- (iii) The Floquet Hamiltonian can be computed theoretically, at least within a suitable approximation valid on the experimentally relevant time scale, and takes a simple form that allows for a clear interpretation.

The first two requirements make ultracold atomic quantum gases, which are well isolated from their environment and provide a great freedom for time dependent parameter control, an optimal platform for Floquet engineering.

Based on this strategy it is also possible to endow a system with qualitatively new properties. A prime example is the creation of artificial gauge fields (magnetic fields or spin orbit coupling), which among others (Dalibard *et al.*, 2011; Galitski and Spielman, 2013; Goldman *et al.*, 2014) can be accomplished using Floquet engineering. For that purpose charge-neutral atoms in an optical lattice are driven in such a way that they behave effectively as if they had a charge coupling to a magnetic field or to their spin. Such a proposal for the realization of an artificial magnetic field was first made by Sørensen *et al.*, 2005, based on a sequence of overlapping pulses during each cycle where external potentials and the amplitudes of the tunneling matrix elements in both directions are switched on in an alternating fashion. Later, simpler schemes, relying solely on the modulation of on-site potentials, were realized experimentally. This includes the effective creation of a topologically non-trivial band structure by means of circular forcing (Oka and Aoki, 2009), known as *Floquet topological insulator* (see also the related work by Kitagawa *et al.*, 2010 and Lindner *et al.*, 2012). Originally proposed for electrons in irradiated graphene, it was realized with fermionic atoms in a circularly shaken honeycomb-like lattice (Jotzu *et al.*, 2014) [as well as in an optical wave-guide experiment (Rechtsman *et al.*, 2013)]. Lattice shaking was also employed to create kinetic frustration and staggered magnetic fields in a triangular optical lattice (Eckardt *et al.*, 2010; Struck *et al.*,

¹ In this high-frequency limit the phenomenon is equivalent to the effective modification of the Landé factor of an off-resonantly driven atomic spin (Haroche *et al.*, 1970) and the effect of *coherent destruction of tunneling* (Grossmann *et al.*, 1991) in a driven two-level system (Gomez Llorente and Plata, 1992; Grifoni and Hänggi, 1998; Grossmann and Hänggi, 1992; Shirley, 1965) observed in an atom-beam experiment (Kierig *et al.*, 2008).

² Let us make a note on terminology: The Floquet Hamiltonian, as it is defined here, is a special case of an effective Hamiltonian \hat{H}_F introduced in Eq. (4) below [see Eq. (11) and the paragraph containing it]. It is also called “effective Hamiltonian” by some authors. Moreover, the term “Floquet Hamiltonian” is sometimes used to denote the operator $\hat{Q}(t) = \hat{H}(t) - i\hbar d_t$ [Eq. 69] acting in the space of time-periodic states, which will be denoted “quasienergy operator” here.

2011, 2012, 2013). Finally, the effective creation of magnetic fields can be achieved in a square lattice where tunneling against strong potential offsets is resonantly induced by driving the system with a moving secondary lattice (Bermudez *et al.*, 2011; Kolovsky, 2011), as has been demonstrated experimentally with bosonic atoms (Aidelsburger *et al.*, 2013, 2011, 2015; Atala *et al.*, 2014; Kennedy *et al.*, 2015; Miyake *et al.*, 2013).

Despite these experimental results, which reflect the great success of Floquet engineering in atomic quantum gases, it would be misleading to state that the stroboscopic time evolution of periodically driven quantum systems simply corresponds to that of some effective autonomous (*i.e.* non-driven) system. Even though we can define a Floquet Hamiltonian $\hat{H}_{t_0}^F$, its properties are generally quite different from those of the time-independent Hamiltonians used to describe autonomous many-body systems. These differences result from the absence of energy conservation in the driven systems, which is reflected in the fact that the Floquet Hamiltonian is not defined uniquely by the relation (1). Namely, its eigenvalues, the *quasienergies*, are determined modulo the energy quantum $\hbar\omega$ only; the quasienergy spectrum can be represented on a circle. Thus, when switching on a time-periodic perturbation, eigenstates of the unperturbed time-independent Hamiltonian with energies separated by some integer multiple of $\hbar\omega$ can hybridize. The eigenstates of $\hat{H}_{t_0}^F$ can, therefore, be coherent superpositions of unperturbed states of rather different energy. In the above-mentioned experiments such resonant coupling plays two different roles. On the one hand it is sometimes exploited to induce coherent tunneling against static potential offsets of integer multiples of $\hbar\omega$ and plays a major role for engineering desired system properties. On the other hand, it also causes heating. For the purpose of Floquet engineering such heating has to be suppressed on the experimentally relevant time scale by a suitable choice of parameters. Further fundamental differences between the (stroboscopic) dynamics of periodically driven quantum systems and that of autonomous systems, like the possible emergence of anomalous topological edge states or the response to slow parameter variations, will be discussed in Section IV.

This article reviews the status of Floquet engineering in systems of ultracold atomic quantum gases in periodically driven optical lattices. For this purpose, we will first briefly summarize a few general properties of time-periodically driven quantum systems in section II. In section III we will then describe recent experiments and explain them in terms of a common language and using simple intuitive approximations. This section addresses also readers who are not interested in the formalism of Floquet theory. This formalism, the *Floquet picture*, will then be introduced in section IV and employed to describe various effects beyond the simple approximations used in the preceding section III. Here we will discuss

issues like those mentioned in the previous paragraph: heating, the asymptotic behavior in the long-time limit, anomalous topological edge states, and the effective adiabatic dynamics required for state preparation. We will close with conclusion and outlook in section V.

The material and the references covered in the present article are selected as follows. We try to give a rather complete overview of the recent experiments, where periodic forcing was used to coherently control atomic quantum gases in optical lattices (not including experiments where modulation was employed for spectroscopic purposes). This includes the corresponding theoretical proposals and analyses. The theory of periodically driven many-body quantum systems recently became an active field. We do not attempt to (and cannot) give an exhaustive overview of this rapidly growing field, but mention some pioneering contributions relevant for future quantum-gas experiments. This selection of covered works reflects the interests and the background of the author and is constrained by the format of a short review. It unavoidably misses contributions that would have been worth being covered as well. Further information and references about the Floquet theory of periodically driven quantum systems can be found in recent review articles, covering the control of tunneling (Grifoni and Hänggi, 1998), multiphoton processes in atoms and molecules (Chu and Telnov, 2003), AC-driven transport in nano-structured devices (Kohler *et al.*, 2005; Platero and Aguado, 2004), the high-frequency regime (Bukov *et al.*, 2015a; Goldman and Dalibard, 2014) and band-structure engineering (Holthaus, 2016).

II. SOME GENERAL PROPERTIES OF FLOQUET SYSTEMS

Let us consider quantum systems described by a time-periodic Hamiltonian

$$\hat{H}(t) = \hat{H}(t + T) = \sum_{m=-\infty}^{\infty} e^{im\omega t} \hat{H}_m, \quad (2)$$

with $\hat{H}_m \equiv \frac{1}{T} \int_0^T dt e^{-im\omega t} \hat{H}(t) = \hat{H}_{-m}^\dagger$. The time evolution operator $\hat{U}(t, t_0)$ describes solutions $|\psi(t)\rangle = \hat{U}(t, t_0)|\psi(t_0)\rangle$ of the time-dependent Schrödinger equation

$$i\hbar d_t |\psi(t)\rangle = \hat{H}(t) |\psi(t)\rangle. \quad (3)$$

At least formally, one can now construct a time-periodic unitary operator $U_F(t) = \hat{U}_F(t + T)$, such that the time evolution of the transformed state $|\psi_F(t)\rangle = \hat{U}_F^\dagger(t) |\psi(t)\rangle$

is governed by a *time-independent* Hamiltonian³

$$\hat{H}_F = \hat{U}_F^\dagger(t) \hat{H}(t) \hat{U}_F(t) - i\hbar \hat{U}_F^\dagger(t) \dot{\hat{U}}_F(t). \quad (4)$$

In terms of these operators, the time evolution operator takes the form (Shirley, 1965)

$$\hat{U}(t, t_0) \equiv \hat{U}_F(t) \exp\left(-\frac{i}{\hbar}(t - t_0) \hat{H}_F\right) \hat{U}_F^\dagger(t_0). \quad (5)$$

It illustrates that the evolution of a Floquet system results from the interplay of two ingredients. On the one hand, the *micromotion operator* $\hat{U}_F(t)$ describes a time-periodic component of the dynamics, the micromotion. It can also be expressed like $\hat{U}_F(t) = e^{-i\hat{K}(t)}$ in terms of a hermitian time-periodic *kick operator* $\hat{K}(t)$. On the other hand, the time-independent *effective Hamiltonian* \hat{H}_F describes a linear phase evolution, which determines the time evolution in a similar way as a time-independent Hamiltonian determines the time evolution of an autonomous system.

The eigenvalue problem of the effective Hamiltonian

$$\hat{H}_F |\tilde{u}_n\rangle = \varepsilon_n |\tilde{u}_n\rangle \quad (6)$$

gives rise to generalized stationary states $|\psi_n(t)\rangle$ of the time dependent Schrödinger equation, called *Floquet states*. They are of the form (Autler and Townes, 1955; Shirley, 1965; Zel'dovich, 1967)

$$|\psi_n(t)\rangle = e^{-\frac{i}{\hbar}t\varepsilon_n} |u_n(t)\rangle, \quad |u_n(t)\rangle = \hat{U}_F(t) |\tilde{u}_n\rangle. \quad (7)$$

Here the periodic time-dependence of the *Floquet mode* $|u_n(t)\rangle = |u_n(t + T)\rangle$ represents the micromotion and the quasienergy ε_n determines the linear phase evolution. The Floquet states are eigenstates of the time-evolution operator over one driving period,

$$|\psi_n(t + T)\rangle = \hat{U}(t + T, t) |\psi_n(t)\rangle = e^{-\frac{i}{\hbar}T\varepsilon_n} |\psi_n(t)\rangle. \quad (8)$$

For every time t , they form a complete and orthogonal basis. If the system is prepared in a Floquet state, its time evolution is periodic, determined by the Floquet mode $|u_n(t)\rangle$, and in this sense quasi stationary. If the system is prepared in a coherent superposition of several Floquet states,

$$|\psi(t)\rangle = \sum_n c_n e^{-\frac{i}{\hbar}t\varepsilon_n} |u_n(t)\rangle, \quad c_n = e^{\frac{i}{\hbar}t_0\varepsilon_n} \langle u_n(t_0) | \psi(t_0) \rangle, \quad (9)$$

deviations from a periodic evolution are governed by the quasienergies ε_n .

There is not a unique time-periodic micromotion operator $\hat{U}_F(t)$ leading to a unique time-independent effective Hamiltonian \hat{H}_F . Starting from one solution, $\hat{U}_F(t)$, another one, $\hat{U}'_F(t)$, can be constructed by applying certain operations. The Floquet states $|\psi_n(t)\rangle$, being eigenstates of the time-evolution operator, will not be altered by such operations. The simplest possibility is to multiply the micromotion operator with an arbitrary time-independent unitary operator \hat{U} from the right, $\hat{U}'_F(t) = \hat{U}_F(t) \hat{U}$, so that $\hat{H}'_F = \hat{U}^\dagger \hat{H}_F \hat{U}$. For example, by choosing $\hat{U}'_F(t) = \hat{U}_F(t) \hat{U}_F^\dagger(t_0) \equiv \hat{U}_F(t, t_0)$ a new micromotion operator is obtained that becomes equal to the identity once during each driving period, $\hat{U}'_F(t_0) = \hat{U}_F(t_0, t_0) = 1$. This allows for writing the time-evolution operator like

$$\hat{U}(t, t_0) \equiv \hat{U}_F(t, t_0) \exp\left(-\frac{i}{\hbar}(t - t_0) \hat{H}_F^F\right), \quad (10)$$

with *Floquet Hamiltonian*

$$\hat{H}_F^F = \hat{U}_F(t_0) \hat{H}_F \hat{U}_F^\dagger(t_0) \quad (11)$$

and *two-point micromotion operator*

$$\hat{U}_F(t, t_0) = \hat{U}_F(t) \hat{U}_F^\dagger(t_0). \quad (12)$$

In particular, for $t = t_0 + T$ Eq. (10) reduces to Eq. (1). The Floquet Hamiltonian is a special choice of the effective Hamiltonian, which directly generates the stroboscopic time evolution in steps of the driving period T . \hat{H}_F^F depends parametrically on the initial time t_0 , and thus also on the driving phase. However, according to Eq. (11) this dependence is rooted in a unitary transformation, so that the spectrum of the Floquet Hamiltonian is independent of t_0 and the driving phase.

Another possibility to construct a new micromotion operator and effective Hamiltonian is given by $\hat{U}'_F(t) = \hat{U}_F(t) \exp(im\omega t |\tilde{u}_n\rangle \langle \tilde{u}_n|)$ with integer m , which implies $\hat{H}'_F = \hat{H}_F + m\hbar\omega |\tilde{u}_n\rangle \langle \tilde{u}_n|$. This operation changes the quasienergy ε_n and its Floquet mode to new solutions labeled by m :

$$\varepsilon_{nm} = \varepsilon_n + m\hbar\omega, \quad |u_{nm}(t)\rangle = e^{im\omega t} |u_n(t)\rangle, \quad (13)$$

such that the corresponding Floquet state is not altered,

$$|\psi_n(t)\rangle = e^{-\frac{i}{\hbar}t\varepsilon_n} |u_n(t)\rangle = e^{-\frac{i}{\hbar}t\varepsilon_{nm}} |u_{nm}(t)\rangle. \quad (14)$$

Equation (13) shows that quasienergies are defined up to integer multiples of $\hbar\omega$ only, in agreement with the earlier observation that Eq. (1) does not determine the Floquet Hamiltonian uniquely. This property reflects the possibility of resonant coupling. The freedom to choose m individually for each Floquet state n , can be used to choose all quasienergies to lie in the same interval of width $\hbar\omega$. Such an interval is often called *Brillouin zone*, in loose analogy to Bloch's theory of spatially periodic

³ Such a transformation might not exist in the limit of an infinite-dimensional states space (Gesztesy and Mitter, 1981). However, here we are dealing with systems of finite spatial extent on finite time scales, on which states above some high-energy cutoff will not matter.

systems. In the latter quasimomenta are defined modulo reciprocal lattice vectors only. They can be chosen to lie in one elementary cell of the reciprocal lattice such as the first Brillouin zone. In case the Floquet mode $|u_n(t)\rangle \equiv \sum_{m'} |u_n^{(m')}\rangle e^{-im'\omega t}$ is dominated by a specific harmonic $m' = m_0$ with respect to a given frame of reference, $m = m_0$ constitutes a meaningful choice for the quasienergy, which, in the limit of a time-independent Hamiltonian, reproduces the energy spectrum.

A prerequisite for Floquet engineering is a theoretical method to compute the effective Hamiltonian and the micromotion operator, at least within a suitable approximation. For $\hbar\omega$ large compared to the matrix elements of the Hamiltonian, a systematic approximation to the effective Hamiltonian and the micromotion operator is given by a high-frequency expansion (Eckardt and Anisimovas, 2015; Goldman and Dalibard, 2014; Goldman *et al.*, 2015; Grozdanov and Raković, 1988; Itin and Katsnelson, 2014; Mikami *et al.*, 2016; Rahav *et al.*, 2003))

$$\hat{H}_F \approx \sum_{\mu=1}^{\mu_{\text{cut}}} \hat{H}_F^{(\mu)}, \quad \hat{U}_F(t) \approx \exp\left(\sum_{\mu=1}^{\mu_{\text{cut}}} \hat{G}^{(\mu)}(t)\right). \quad (15)$$

Here $\hat{H}_F^{(\mu)\dagger} = \hat{H}_F^{(\mu)}$ and $[\hat{G}^{(\mu)}(t)]^\dagger = -\hat{G}^{(\mu)}(t)$. The leading terms are given by

$$\begin{aligned} \hat{H}_F^{(1)} &= \hat{H}_0, & \hat{H}_F^{(2)} &= \sum_{m \neq 0} \frac{\hat{H}_m \hat{H}_{-m}}{m\hbar\omega}, \\ \hat{H}_F^{(3)} &= \sum_{m \neq 0} \left[\frac{[\hat{H}_{-m}, [\hat{H}_0, \hat{H}_m]]}{2(m\hbar\omega)^2} \right. \\ &\quad \left. + \sum_{m' \neq 0, m} \frac{[\hat{H}_{-m'}, [\hat{H}_{m'-m}, \hat{H}_m]]}{3mm'(\hbar\omega)^2} \right], \end{aligned} \quad (16)$$

and

$$\begin{aligned} \hat{G}^{(1)}(t) &= -\sum_{m \neq 0} \frac{e^{im\omega t} \hat{H}_m}{m\hbar\omega}, \\ \hat{G}^{(2)}(t) &= \sum_{m \neq 0} \left[\frac{e^{im\omega t} [\hat{H}_0, \hat{H}_m]}{(m\hbar\omega)^2} \right. \\ &\quad \left. + \sum_{m' \neq 0, m} \frac{e^{i(m-m')\omega t} [\hat{H}_{-m'}, \hat{H}_m]}{2m(m-m')(\hbar\omega)^2} \right]. \end{aligned} \quad (17)$$

A similar high-frequency expansion for the Floquet Hamiltonian $\hat{H}_{t_0}^F$ and the two-point micromotion operator $\hat{U}_F(t, t_0)$ is known as Floquet-Magnus expansion (Blanes *et al.*, 2009; Bukov *et al.*, 2015a; Casas *et al.*, 2000; Maricq, 1982; Milfeld and Wyatt, 1983; Verdeny *et al.*, 2013)

$$\hat{H}_{t_0}^F \approx \sum_{\mu=1}^{\mu_{\text{cut}}} \hat{H}_{t_0}^{F(\mu)}, \quad \hat{U}_F(t, t_0) \approx \exp\left(\sum_{\mu=1}^{\mu_{\text{cut}}} \hat{F}^{(\mu)}(t, t_0)\right). \quad (18)$$

We can contract the leading terms from the expansion (15) using Eqs. (11) and (12). For the Floquet-Hamiltonian they read

$$\begin{aligned} \hat{H}_{t_0}^{F(1)} &= \hat{H}_F^{(1)} = \hat{H}_0, \\ \hat{H}_{t_0}^{F(2)} &= \hat{H}_F^{(2)} - [\hat{H}_F^{(1)}, G^{(1)}(t_0)] \\ &= \sum_{m \neq 0} \frac{\hat{H}_m \hat{H}_{-m} + e^{im\omega t_0} [H_0, H_m]}{m\hbar\omega}. \end{aligned} \quad (19)$$

Here the second term of $\hat{H}_{t_0}^{F(2)}$ results from the expansion of the unitary operator $\hat{U}_F(t) \simeq 1 + \hat{G}^{(1)}(t) + \dots$. This expansion conserves unitarity only up to the considered order μ_{cut} , e.g. in first order one finds $[1 + \hat{G}^{(1)}(t)]^\dagger [1 + \hat{G}^{(1)}(t)] = 1 - [\hat{G}^{(1)}(t)]^2$. As a consequence, the approximate quasienergy spectrum obtained from the Floquet Hamiltonian in μ_{cut} th-order acquires a spurious dependence on the initial time t_0 and, thus, also on the driving phase. When expanding the spectrum in powers of the inverse driving frequency, the t_0 dependence appears in terms of powers $\geq \mu_{\text{cut}}$, which cannot be expected to be captured correctly within the given order of the approximation. While these terms should be small in the regime where the approximation is justified, they might cause spurious symmetry breaking (Eckardt and Anisimovas, 2015).

The Floquet-Magnus expansion is guaranteed to converge, if the period-averaged operator norm of the Hamiltonian $\hat{H}(t)$ is smaller than $\xi_F \hbar\omega$, where ξ_F is a constant of order one (Casas *et al.*, 2000). For periodically driven many-body systems, possessing excited states also at macroscopically large energies, this condition cannot be expected to be fulfilled (unless the state space is effectively reduced by symmetry or localization). However, even in this case the high-frequency expansion might still provide a suitable approximation provided $\hbar\omega$ is large compared to the typical intensive energy scales of the system, at least up to a certain time span t_h beyond which the system heats up (Abanin *et al.*, 2014; Kuwahara *et al.*, 2016; Maricq, 1982; Mori *et al.*, 2016). Abanin *et al.*, 2014 and Kuwahara *et al.*, 2016 showed that for spin systems with local interactions (i.e. for systems with local energy bound) the time scale t_h increases exponentially with the driving frequency. For these systems, Kuwahara *et al.*, 2016, moreover, showed that for time spans smaller than t_h the Floquet-Magnus expansion is (at least) an asymptotic series that provides a good approximation for the time-evolution operator, whose error rapidly decreases with μ_{cut} before it increases again beyond an optimal order $\mu_{\text{cut}}^{\text{opt}}$. While these results do not apply to optical lattice systems, which do not have a local energy bound, they still indicate that the high-frequency approximation can provide an accurate description of a driven many-body system as long as the duration of the experiment is short compared to some heating time t_h . This issue is discussed in more detail in section IV.

The approximate effective Hamiltonian, as it is given by a certain low order μ_{cut} of the high-frequency approximation (15), defines a simple model Hamiltonian. In contrast, the full effective Hamiltonian of a driven system of many interacting particles is typically a highly complex (rather awkward) object, which cannot be written down explicitly. Very often the starting point of Floquet engineering is, therefore, to realize the physics of an autonomous model described by a target Hamiltonian \hat{H}_{target} directly corresponding to the high-frequency approximation in some low order ($\mu_{\text{cut}} = 1$ or 2), $\hat{H}_{\text{target}} = \sum_{\mu=1}^{\mu_{\text{cut}}} \hat{H}_F^{(\mu)}$. From this perspective, the dynamics of the driven quantum system provides an approximation to the physics of the desired model Hamiltonian \hat{H}_{target} , rather than the other way around. The quantum-gas experiments described in the following section III can be interpreted from this point of view.

III. QUANTUM-GAS EXPERIMENTS AND THEIR BASIC DESCRIPTION

This section shall give an overview over recent experiments with quantum gases of ultracold neutral atoms in periodically driven optical lattices. We will not discuss experiments, where periodic driving has been employed for spectroscopic purposes, but rather describe those aiming for the coherent manipulation of the system's state and its dynamics. The observed effects will be explained in terms of a common language and using intuitive approximations.

A. Neutral atoms in optical lattices

Ultracold quantum gases (Bloch *et al.*, 2008; Lewenstein *et al.*, 2012) consist of neutral atoms held in optical or magneto-optical traps inside a vacuum cell and cooled down to quantum degeneracy by means of laser cooling and evaporative cooling. They are very well isolated from their environment. Dissipative processes, such as the formation of molecules via three-body collisions, spontaneous emission as a result of the optical trap, or collisions with background particles, are often negligible. Atom numbers of up to several millions can be reached.

The possibility to create light-shift potentials proportional to the laser intensity allows for the creation of quasi defect-free lattice potentials from standing light waves, called *optical lattices*. For example, a one-dimensional lattice created by two counter-propagating laser beams with wave vectors \mathbf{k}_L and $-\mathbf{k}_L$ takes the form of a cosine lattice, $V_L(\mathbf{r}) = V_0 \sin^2(\mathbf{k}_L \cdot \mathbf{r})$, where the lattice depth V_0 is proportional to the laser intensity. Besides the lattice depth V_0 , a second energy scale is the recoil energy $E_R = \hbar^2 k_L^2 / 2m$, with $k_L = |\mathbf{k}_L|$ and atomic mass m . It corresponds to the kinetic energy required to localize

a particle on the length of a lattice constant $d = \pi/k_L$. Recoil energies are of the order of several ($h \times$) kilohertz, roughly corresponding to ($k_B \times$) microkelvin or several pico-electron volts. The lattice depth can take values of up to hundreds of recoil energies. The rather large time scales corresponding to these low energy scales allow for accurate time-dependent manipulation and time-resolved imaging. By combining standing waves in different direction or by creating more complex interference patterns one can create various two- and three-dimensional lattice structures. Moreover, effectively one- or two-dimensional systems can be realized by strong transversal confinement.

For deep lattices, $V_0 \gg E_R$, the system is well described by a Hubbard model with one localized Wannier state at each lattice minimum. The single-particle terms of the Hamiltonian take the form

$$\hat{H}_{\text{tun}} = - \sum_{\langle \ell' \ell \rangle} J \hat{a}_{\ell'}^\dagger \hat{a}_\ell, \quad \hat{H}_{\text{pot}} = \sum_{\ell} v_\ell \hat{n}_\ell \quad (20)$$

where \hat{a}_ℓ^\dagger , \hat{a}_ℓ , and $\hat{n}_\ell = \hat{a}_\ell^\dagger \hat{a}_\ell$ denote the creation, annihilation and number operator for a particle, boson or fermion, in the Wannier state at lattice site ℓ . The kinetics is captured by \hat{H}_{tun} and to good approximation exhausted by tunneling processes between neighboring sites ℓ and ℓ' , here $\langle \ell' \ell \rangle$ denotes a directed pair of neighboring sites ℓ' and ℓ . The nearest-neighbor tunneling parameter J depends sensitively on the lattice depth and can, depending on the lattice structure, also acquire a directional dependence $J \rightarrow J_{\ell' \ell}$. For a deep cosine lattice $J/E_R \simeq 4\pi^{-1/2} (V_0/E_R)^{3/4} \exp(-2\sqrt{V_0/E_R})$ (Zwenger, 2003). The potential term \hat{H}_{pot} captures the influence of an external potential such as the trap or a superlattice potential.

The interactions among low-temperature alkaline atoms, as they were used in the experiments to be reviewed here, are short-ranged and captured by on-site terms. For spinless bosons the interaction term reads

$$\hat{H}_{\text{int}} = \frac{U}{2} \sum_{\ell} \hat{n}_\ell (\hat{n}_\ell - 1). \quad (21)$$

For deep lattices the Hubbard parameter U approaches $U \simeq \sqrt{2/\pi} \hbar^2 a_s / (m \bar{a}_0^3) = 2E_R \sqrt{2/\pi} (k_L a_s) / (k_L \bar{a}_0)^3$ with s-wave scattering length a_s and the mean harmonic-oscillators length \bar{a}_0 in the lattice minimum. For the cosine lattice the harmonic-oscillator length depends weakly on the lattice depth like $a_0 k_L = (V_0/E_R)^{-1/4}$ and for Rb-87 atoms $k_L a_s \approx 0.041$ at $2\pi/k_L = 850$ nm. Spinless (i.e. spin-polarized) fermions do not interact due to Pauli exclusion. In order to have interactions among fermionic atoms, one has to consider spinful atoms or elements with long-ranged dipolar interactions.

The Hubbard model is justified for sufficiently deep lattices ($V_0/E_R > 5$) and has been tested to provide a quantitative description of optical lattice sys-

tems (Trotzky *et al.*, 2009). Excited states belonging to higher Bloch bands not included in the Hubbard model are separated by a large energy gap E_G of several E_R . The gap E_G , which is roughly given by $E_G \approx E_R \min(V_0/(2E_R), 2\sqrt{V_0/E_R} - 1)$, can be two orders of magnitude larger than J and U . Thus, even if the driving frequency is required to be large compared to J and U , it can still be small compared to the band gap. This suggests that a description of the periodically driven systems in terms of the low-energy subspace described by the Hubbard model is possible. A more detailed discussion of this issue is given in Sec. IV.C below.

B. Dynamic localization

The first experiment where the coherent dynamics of an ultracold quantum gas has been controlled by means of periodic forcing has been conducted in Arimondo's group in Pisa. The ballistic spreading of a localized Bose-Einstein condensate in the lowest band of a one-dimensional optical lattice has been slowed down, and even suppressed completely, by the application of a sinusoidal force (Lignier *et al.*, 2007, see also Creffield *et al.*, 2010 and Eckardt *et al.*, 2009). This is the effect of *dynamic localization* (Dunlap and Kenkre, 1986).

The experimentalists created a one-dimensional optical lattice in the tight-binding regime along the x direction, together with a tube-like harmonic confinement in the radial directions y and z . Initially a Bose-Einstein condensate of ^{87}Rb atoms was loaded into the lowest Bloch band of the lattice, localized in the center of the tube by an additional trapping potential. When this additional trap was switched off, the condensate started to expand in the tube. During this expansion a sinusoidal force was applied, created as an inertial force by shaking the lattice back and forth. The shaken lattice is described by the potential $V_{DL}(\mathbf{r}, t) = V_L(\mathbf{r} - \boldsymbol{\xi}(t))$ with $\boldsymbol{\xi}(t) = \boldsymbol{\xi}(t + T) = \boldsymbol{\xi}(t) = \xi_0 \cos(\omega t) \mathbf{e}_x$, which transforms to $V_L(\mathbf{r}) - \mathbf{r} \cdot \mathbf{F}(t)$ in the reference frame co-moving with the lattice, where

$$\mathbf{F}(t) = -m\ddot{\boldsymbol{\xi}}(t) = \mathbf{F}_\omega \cos(\omega t) \quad (22)$$

with $\mathbf{F}_\omega = m\omega^2 \xi_0 \mathbf{e}_x \equiv F_\omega \mathbf{e}_x$ (Drese and Holthaus, 1997b; Madison *et al.*, 1998). After a certain time of expansion in the driven lattice, the atom density was measured by absorption imaging either *in situ* or, in order to reveal the momentum distribution, after an additional time of flight with all potentials switched off.

For a broad range of parameters, the momentum distribution revealed sharp peaks, indicating that the condensate retained its coherence like in the case of a ballistic expansion and that the shaking did not cause significant heating. Moreover, by comparing the *in-situ* extent of the atom cloud with that found for ballistic expansion in the non-driven lattice (Fig. 1), the driven system was

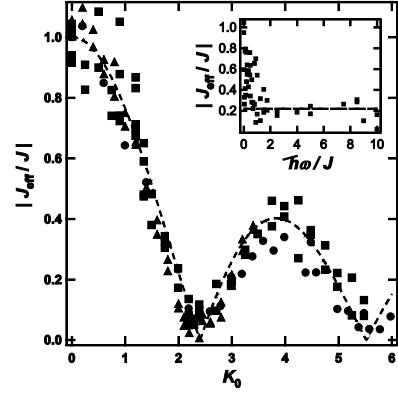


FIG. 1 Effective tunneling matrix element $|J_{\text{eff}}|/J$ versus $K_0 = K/\hbar\omega$. Extracted from the expansion dynamics of a condensate of about $5 \cdot 10^4$ ^{87}Rb atoms in a shaken optical lattice of $E_R \approx 2\pi\hbar 3.16$ kHz (squares: $V_0/E_R = 6$, $\omega/2\pi = 1$ kHz, circles: $V_0/E_R = 6$, $\omega/2\pi = 0.5$ kHz, triangles: $V_0/E_R = 4$, $\omega/2\pi = 1$ kHz, dashed line: theoretical prediction). Inset: J_{eff}/J for $K/\hbar\omega = 2$ and $V_0/E_R = 9$ versus $\hbar\omega/J$, indicates breakdown of high-frequency prediction (dashed line) for $\hbar\omega/J < 2$. (taken from Lignier *et al.*, 2007)

found to be well-described by the effective tunneling parameter predicted by Dunlap and Kenkre, 1986,

$$J_{\text{eff}} = J \mathcal{J}_0\left(\frac{K}{\hbar\omega}\right), \quad (23)$$

where $K = dF_\omega$ is the amplitude of the potential modulation between neighboring lattice sites.

Let us explain this result. In the lattice frame of reference the system can be described by the tight-binding Hamiltonian

$$\hat{H}(t) = - \sum_{\langle \ell' \ell \rangle} J \hat{a}_{\ell'}^\dagger \hat{a}_\ell + \sum_\ell \left[(v_\ell + w_\ell(t)) \hat{n}_\ell + \frac{U}{2} \hat{n}_\ell (\hat{n}_\ell - 1) \right], \quad (24)$$

where ℓ labels the minima $\mathbf{r}_\ell = (x_\ell, 0, 0)$ of the one-dimensional lattice and where

$$w_\ell(t) = -\mathbf{r}_\ell \cdot \mathbf{F}(t) = -\frac{x_\ell}{d} K \cos(\omega t), \quad v_\ell = v_\ell^{\text{tr}} \quad (25)$$

captures the periodic force as well as a weak harmonic trap in the lattice direction v_ℓ^{tr} , respectively. In the expansion experiment v_ℓ^{tr} was small enough to have no significant influence on the measured expansion dynamics.

One can now perform a gauge transformation, $|\psi'(t)\rangle = \hat{U}^\dagger(t) |\psi(t)\rangle$ and $\hat{H}'(t) = \hat{U}^\dagger(t) \hat{H}(t) \hat{U}(t) - i\hbar \hat{U}^\dagger(t) [d_t \hat{U}(t)]$, defined by the time-periodic unitary operator

$$\hat{U}(t) = \exp \left(i \sum_\ell \chi_\ell(t) \hat{n}_\ell \right) \quad (26)$$

with

$$\chi_\ell(t) = - \int_{t_0}^t dt' \frac{w_\ell(t')}{\hbar} - \chi_{0\ell}. \quad (27)$$

The time-independent gauge constant $\chi_{0\ell}$ shall be chosen such that $\int_0^T dt \chi_\ell(t) = 0$. Writing

$$\chi_\ell(t) \equiv \mathbf{r}_\ell \cdot \mathbf{a}(t) \quad (28)$$

reveals that the unitary operator $\hat{U}(t)$ describes a global shift in quasimomentum by

$$\mathbf{a}(t) = -\frac{m}{\hbar} \dot{\boldsymbol{\xi}}(t) = \frac{1}{d} \frac{K}{\hbar \omega} \sin(\omega t) \mathbf{e}_x. \quad (29)$$

By employing $\hat{U}^\dagger(t) \hat{a}_\ell \hat{U}(t) = e^{i\chi_\ell(t)} \hat{a}_\ell$ and noting that the time-derivative of the unitary transformation cancels with the driving term, the gauge-transformed Hamiltonian can be brought to the form

$$\hat{H}'(t) = - \sum_{\langle \ell' \ell \rangle} J e^{i\theta_{\ell' \ell}(t)} \hat{a}_{\ell'}^\dagger \hat{a}_\ell + \sum_\ell \left[v_\ell \hat{n}_\ell + \frac{U}{2} \hat{n}_\ell (\hat{n}_\ell - 1) \right]. \quad (30)$$

The time-dependent Peierls phases

$$\theta_{\ell' \ell}(t) = \chi_\ell(t) - \chi_{\ell'}(t) = -(\mathbf{r}_{\ell'} - \mathbf{r}_\ell) \cdot \mathbf{a}(t) \quad (31)$$

play the role of a discrete vector potential that now, instead of the discrete scalar potential $w_\ell(t)$, describes the force $\mathbf{F}(t)$.

For $v_\ell = 0$, the gauge transform restores the discrete translational symmetry of the lattice. The time-dependent tunneling term of $\hat{H}'(t)$ is, thus, diagonal in quasimomentum representation,

$$\hat{H}'_{\text{tun}}(t) = \sum_{\mathbf{k}} \varepsilon(\mathbf{k} + \mathbf{a}(t)) \hat{n}_{\mathbf{k}}. \quad (32)$$

Here $\hat{n}_{\mathbf{k}}$ denotes the number operator for particles in the Bloch state with quasimomentum wave number \mathbf{k} , characterized by $\langle \ell | \mathbf{k} \rangle \propto \exp(i\mathbf{r}_\ell \cdot \mathbf{k})$, and $\varepsilon(\mathbf{k}) = -2J \cos(dk_x)$ is the single-particle dispersion relation of the undriven tight-binding lattice. The form (32) explicitly shows that the transformation (26) describes a shift in momentum by $\mathbf{a}(t)$.⁴ Under the influence of $\hat{H}'_{\text{tun}}(t)$ the quasimomentum occupation numbers of the state do not change in time. During each driving period a particle in state $|\mathbf{k}\rangle$ just picks up an integrated dynamical phase proportional to the time-averaged energy $\varepsilon_{\text{eff}}(\mathbf{k}) = \frac{1}{T} \int_0^T dt \varepsilon(\mathbf{k} + \mathbf{a}(t)) = -2J_{\text{eff}} \cos(dk_x)$, with the effective tunneling matrix element J_{eff} as given by Eq. (23).⁵ Thus, apart from an oscillatory dynamics at the driving frequency the system behaves as if it was described by the effective dispersion relation $\varepsilon_{\text{eff}}(\mathbf{k})$ with a reduced

band width of $4J_{\text{eff}}$. This argument is valid also for low driving frequencies, unless interactions or translational-symmetry-breaking cause scattering between quasimomentum states.

In the more interesting situation with interactions and translational-symmetry breaking, the effective modification of tunneling is still valid approximately in the high-frequency regime. Namely, if $\hbar\omega$ is large compared to the characteristic energy scales J , U , and $|v_{\ell'} - v_\ell|$ on neighboring sites ℓ' and ℓ , which determine the rates at which the system's state $|\psi'(t)\rangle$ changes in time, we can average over the rapid oscillation of the Peierls phases. The tight-binding Hamiltonian can be approximated by its cycle average

$$\hat{H}'(t) \approx \frac{1}{T} \int_0^T dt \hat{H}'(t) \equiv \hat{H}_{\text{eff}}. \quad (33)$$

One finds

$$\hat{H}_{\text{eff}} = - \sum_{\langle \ell' \ell \rangle} J_{\ell' \ell}^{\text{eff}} \hat{a}_{\ell'}^\dagger \hat{a}_\ell + \sum_\ell \left[v_\ell \hat{n}_\ell + \frac{U}{2} \hat{n}_\ell (\hat{n}_\ell - 1) \right], \quad (34)$$

with modified tunneling matrix element

$$J_{\ell' \ell}^{\text{eff}} = \frac{J}{T} \int_0^T dt e^{i[\chi_\ell(t) - \chi_{\ell'}(t)]}, \quad (35)$$

resulting in $J_{\ell' \ell}^{\text{eff}} = J_{\text{eff}}$, where J_{eff} is given by Eq. (23).⁶ This rotating-wave-type approximation is in principle valid not only for the case of weak interactions of the expansion experiment, but also in the regime where U is comparable or larger than J (Eckardt *et al.*, 2005).

The result of the rotating-wave approximation can be related to Floquet theory. The time-independent Hamiltonian \hat{H}_{eff} that was argued to effectively describe the time evolution, constitutes an approximation to the effective Hamiltonian \hat{H}_F and the unitary operator (26) approximates the micromotion operator $\hat{U}_F(t)$:

$$\hat{H}_F \approx \hat{H}_{\text{eff}}, \quad \hat{U}_F(t) \approx \hat{U}(t). \quad (36)$$

This corresponds to the leading order of the high-frequency approximation (15) applied to $\hat{H}'(t)$,

$$\hat{H}_{\text{eff}} = \hat{H}_F^{(1)}. \quad (37)$$

As will be discussed in section IV this approximation is expected to be valid on a certain time scale, before heating sets in. This time scale can, however, be rather long and comparable to the duration of the experiment (typically a few hundred milliseconds). In the experiment by Lignier *et al.*, 2007, the condensate coherence

⁴ The transformation can be viewed as an analog of the Kramers-Henneberger transformation (Henneberger, 1968), with the roles of momentum and position interchanged.

⁵ In order to compute the time average, the identity $\exp(ia \sin(b)) = \sum_{\mu=-\infty}^{\infty} \mathcal{J}_\mu(a) \exp(i\mu b)$ was employed.

⁶ For non-sinusoidal square-wave forcing the modification of tunneling is given by a sinc function (Zhu *et al.*, 1999), as it was observed also experimentally (Eckardt *et al.*, 2009).

was found to decay during the expansion on a dephasing time of about 200 milliseconds for the non-driven system with $V_0/E_R \approx 9$. For the strongly driven system with $K/\hbar\omega = 2.2$ comparable dephasing times were achieved when the driving frequency was increased to an optimal value.

A significant modification of tunneling requires strong driving with the driving strength K of the order of $\hbar\omega$. For such strong forcing it would not have been justified to approximate the original Hamiltonian $\hat{H}(t)$ by its time average, since the amplitude of the driving term K changes the state at a rate comparable to the driving frequency. However, by integrating out the driving term via a gauge transformation before applying the rotating-wave approximation, also the case of strong driving can be treated (Eckardt *et al.*, 2010; Goldman *et al.*, 2015). In this way a non-perturbative treatment of the forcing has been achieved. This is visible in the fact that through the Bessel-function-type dependence the effective tunneling matrix element J_{eff} contains arbitrarily large powers of the driving amplitude K . In contrast, when performing the high-frequency expansion starting from $\hat{H}(t)$ in μ th order the largest power encountered is K^μ . Thus, integrating out the driving term via the gauge transformation (26) before employing the high-frequency expansion corresponds to a partial resummation of the series (15).

Lignier *et al.*, 2007 also observed deviations from the tight-binding description (24) in the form of a small amount of transfer to the first excited band of the lattice (less than ten percent for $K/\hbar\omega < 3$). Moreover, for negative effective tunneling matrix elements $J_{\text{eff}} < 0$, the measured momentum distribution revealed that the atoms recondensed into the minimum $k_x = \pi/d$ of the inverted dispersion relation $\varepsilon_{\text{eff}}(\mathbf{k})$. A plausible explanation of this process, during which the (effective) kinetic energy is lowered, is that the excess energy is absorbed by excitations in the rather weakly confined transversal direction.

The fact that the periodic force has been created as an inertial force via lattice shaking has a convenient implication concerning the measurement of the quasimomentum distribution. In the lattice frame of reference the quasimomentum distribution oscillates like $-\mathbf{a}(t)$ in response to the inertial force. This oscillation is removed, when transforming back to the laboratory frame of reference, where the quasimomentum distribution is measured. This resembles the effect of the gauge transformation that led to $\hat{H}'(t) \approx \hat{H}_{\text{eff}}$. Time-of-flight pictures, thus, directly reveal the quasimomentum distribution of \hat{H}_{eff} (multiplied, however, by an oscillating envelop given by the Fourier transform of the Wannier function).

C. “Photon”-assisted coherent tunneling

The starting point of a second type of experiment has been the Wannier-Stark configuration, namely a one-dimensional lattice system in combination with a homogeneous static force $\mathbf{F}_0 = F_0 \mathbf{e}_x$. If the potential difference between neighboring sites $\Delta = F_0 d$ is large compared to the band width (while still being small with respect to the band gap) tunneling processes between neighboring lattice sites are strongly suppressed. In this regime the localized single-particle Wannier-Stark eigenstates are approximately identical to the Wannier states at the lattice sites ℓ , and Bloch oscillations are reduced to a rapid shivering motion of angular frequency Δ/\hbar and negligible amplitude $\sim J/\Delta$. An initially localized Bose condensate does not spread in time. However, coherent tunneling can be induced by applying a time-periodic force $\mathbf{F}_\omega \cos(\omega t)$, provided the resonance condition

$$\Delta = \nu \hbar \omega + \delta, \quad (38)$$

with integer ν and small detuning δ is met. This phenomenon is known as “photon”-assisted, AC-induced, or laser-assisted tunneling. For such a situation the energy separation Δ between neighboring sites is bridged by ν energy quanta $\hbar\omega$ (tunneling corresponds to an allowed ν -“photon” transition) and particles can tunnel with an effective tunneling matrix element $-J_{\text{eff}}$, as if there was no potential tilt (Zak, 1993).

If the resonance condition is not met exactly such that a finite detuning δ remains, this detuning plays the role of a residual static force $\delta \mathbf{F} = (\delta/d) \mathbf{e}_x$ (Eckardt and Holthaus, 2007). If δ is comparable or small with respect to the AC-induced tunneling matrix element J_{eff} , it can lead to significant coherent Bloch oscillations of angular frequency δ/\hbar , either in the form of a periodic breathing dynamics, as observed by Alberti *et al.*, 2009, in Florence, or in the form of a periodic center of mass motion, as in the Innsbruck experiment by Haller *et al.*, 2010. The latter phenomenon has been coined *super Bloch oscillations* by Kolovsky and Korsch, 2010.

A basic theoretical description of “photon”-assisted tunneling in a sinusoidally forced tilted lattice can be obtained in a similar way as for the phenomenon of dynamic localization. Subjecting a one-dimensional lattice system to the force

$$\mathbf{F}(t) = -\mathbf{F}_0 + \mathbf{F}_\omega \cos(\omega t), \quad (39)$$

with $\mathbf{F}_0 = F_0 \mathbf{e}_x$ and $\mathbf{F}_\omega = F_\omega \mathbf{e}_x$, it is described by the Bose-Hubbard Hamiltonian (24). However now the driving potential is defined like

$$w_\ell(t) = \frac{x_\ell}{d} [-K \cos(\omega t) + \nu \hbar \omega], \quad (40)$$

where $K = F_\omega d$ as before, and

$$v_\ell = v_\ell^{\text{tr}} + \frac{x_\ell}{d} \delta, \quad (41)$$

describes an additional weak static potential. Here we have included the larger share $\nu\hbar\omega$ of the static potential tilt (38) to the *driving term* $w_\ell(t)$, whereas the small detuning δ was included into v_ℓ .

Now $w_\ell(t)$ contains all terms of the Hamiltonian, whose characteristic energy scale is not small compared to the driving frequency. Moreover the $w_\ell(t)$ term is defined such that it can be integrated out by a time-periodic gauge transformation, described by the unitary operator (26) and (27) with $w_\ell(t)$ as defined by Eq. (40). This gauge transformation leads to a Hamiltonian of the form (30). It corresponds to a global shift in quasimomentum by

$$\mathbf{a}(t) = \left[\frac{1}{d} \frac{K}{\hbar\omega} \sin(\omega t) - \frac{1}{d} \nu \omega t + a_0 \right] \mathbf{e}_x, \quad (42)$$

where the constant a_0 depends both on the integration time t_0 and the gauge constant $\chi_{0\ell}$ in Eq. (27). The linear dependence on time makes the definition of $\chi_{0\ell}$ as the time average of the integral in Eq. (27) meaningless. Instead the freedom to choose $\chi_{0\ell}$ can be used either to achieve $a_0 = 0$ for convenience, as shall be done in the following, or to incorporate into a_0 the actual momentum shift induced when both \mathbf{F}_ω and \mathbf{F}_0 are switched on according to a particular experimental protocol. The quasimomentum shift (42) is time periodic, in the sense that quasimomentum wave numbers k_x are defined modulo $\frac{2\pi}{d}$ only. The integer ν corresponds to the number of times the system is translated in quasimomentum through the first Brillouin zone.

We are now again in the position to approximate $\hat{H}'(t) = \hat{H}'(t + T)$ by its time average, as long as J , U , and $|v_{\ell'} - v_\ell|$ on neighboring sites ℓ' and ℓ (i.e. also $|\delta|$) are small compared to $\hbar\omega$. We arrive at the approximate effective Hamiltonian (34), but with v_ℓ given by Eq. (41) and with the effective tunneling matrix element reading (Eckardt and Holthaus, 2007; Zak, 1993)

$$J_{\text{eff}} = J \mathcal{J}_\nu \left(\frac{K}{\hbar\omega} \right). \quad (43)$$

For small arguments the Bessel function behaves like $\mathcal{J}_\nu(x) \simeq \frac{1}{|\nu|!} [\text{sgn}(\nu) \frac{x}{2}]^{|\nu|}$, so that for $\nu \neq 0$ the effective tunneling matrix element vanishes for $K/\hbar\omega = 0$. This reflects the fact that for a strong potential tilt $\nu\hbar\omega \gg J$ tunneling is suppressed. However, switching on a finite driving strength $K/\hbar\omega$ the effective tunneling matrix element acquires finite values such that coherent “photon”-assisted tunneling is induced by the periodic force.

The fact that the localized Wannier-Stark eigenstates of the tight-binding model described by \hat{H}_{eff} with a finite tilt δ are known explicitly in the absence of trapping potentials and interactions, allows for an analytical description of the dynamics of an initially localized wave packet in the shaken tilted lattice (Thommen *et al.*, 2002, 2004a,b, see also Kolovsky and Korsch, 2010 and Kudo

and Monteiro, 2011), as it has been investigated in different experiments to be described in the following paragraphs.

“Photon”-assisted tunneling described by the effective tunneling matrix element (43) with $\nu = 1$ and $\nu = 2$ has been observed in Arimondo’s group in Pisa (Sias *et al.*, 2008) from the coherent expansion of a Bose condensate of Rb-87 atoms in a one-dimensional lattice, where both the static and the sinusoidal force were created by lattice acceleration [a seeming discrepancy between the measured data with the prediction (43) was later resolved by taking into account the initial extent of the condensate when extracting the effective tunneling matrix element (Creffield *et al.*, 2010)].

At the same time a similar experiment has been conducted in Tino’s group in Florence with Sr-88 atoms in an optical cosine lattice, where the static force was given by gravitation and the periodic force was realized via lattice shaking (Ivanov *et al.*, 2008). The experimentalists observed ballistic spreading for resonant forcing with $\hbar\omega = n\Delta$ and $n = 1, 2, 3$ and 4. The authors attribute the resonances to tunneling processes between lattice sites at distance nd . Since for the used lattice depth of $V_0/E_R = 20$ the matrix elements for next-nearest-neighbor tunneling are negligible, this interpretation suggests that atoms were loaded also into excited Bloch bands of the lattice, where also longer-ranged tunneling matrix elements matter. An alternative mechanism leading to such resonances would be n th-order tunneling processes, where n particles tunnel to a neighboring site via virtual intermediate non-resonant states.

In a later experiment by the same group the atoms were loaded into the lowest band of a tilted lattice and the impact of the small effective lattice tilt $\delta = \Delta - \hbar\omega$ was explored, as it appears in the effective Hamiltonian (34) through v_ℓ [Eq. (41)]. The experimentalists observed a large-amplitude breathing dynamics of the initially localized atom cloud at the small effective Bloch frequency $\delta/(2\pi\hbar)$ (Alberti *et al.*, 2009). For the lowest effective Bloch frequency of approximately 0.26 Hertz a breathing amplitude of about one millimeter was observed. The driven system retained coherence over *macroscopic* times and distances. Since the atom cloud was hot, with the momentum distribution smeared out over the whole first Brillouin zone, no center-of-mass Bloch oscillations were observed. However, the thermal nature of the initial state did not destroy the coherent breathing dynamics.

In an experiment by Nägerl’s group in Innsbruck also center-of mass oscillations at the effective Bloch frequency $\delta/(2\pi\hbar)$ were observed (Haller *et al.*, 2010). In this experiment with bosonic Cs-133 atoms in a one-dimensional optical lattice the static tilt was given by gravitation and the sinusoidal force was realized using an oscillating magnetic-field gradient. Since the atom cloud possessed a peaked quasimomentum distribution, it acquired also a large-amplitude center of mass oscillation

(super Bloch oscillations), described by the group velocity of the effective Hamiltonian at the oscillating quasimomentum peak. The amplitude of the oscillations was found to be determined by J_{eff} as given by Eq. (43) with $\nu = 1$. Their phase, as it is determined by the quasimomentum shift acquired while the forcing is switched on, was controlled by the time when during the driving period the forcing was switched on abruptly.

Another possibility to resonantly induce effective coherent tunneling in a strongly tilted lattice is a sinusoidal modulation of the lattice depth, which is captured by a modulation of the tunneling matrix element in the tight-binding Hamiltonian (24),

$$J \rightarrow J(t) = \sum_{\mu=-\infty}^{\infty} J^{(\mu)} e^{i\mu\omega t} \simeq J + \Delta J \cos(\omega t), \quad (44)$$

with $J^{(-\mu)} = J^{(\mu)*}$. Additionally, there is also a weak periodic modulation of the interaction parameter, $U \rightarrow U(t) \simeq U - \Delta U \cos(\omega t)$. The Wannier-Stark tilt is captured by

$$w_\ell = \frac{x_\ell}{d} \nu \hbar \omega, \quad v_\ell = v_\ell^{\text{tr}} + \frac{x_\ell}{d} \delta. \quad (45)$$

Integrating out the strong potential tilt included in w_ℓ by a gauge transformation [Eqs. (26) and (27)], one arrives at a Hamiltonian $\hat{H}'(t)$ of the form (30), with J and U replaced by $J(t)$ and $U(t)$ and Peierls phases (31) determined by the quasimomentum shift

$$\mathbf{a}(t) = [-\frac{1}{d} \nu \omega t + a_0] \mathbf{e}_x. \quad (46)$$

Once again, one can approximate $\hat{H}'(t)$ by its time average, giving the effective Hamiltonian (34), where v_ℓ is given by Eq. (45) and where for the choice of gauge $a_0 = 0$ the effective tunneling matrix element reads

$$J_{\text{eff}} = J^{(-\nu_{\ell'\ell})} \simeq \delta_{\nu,0} J + \frac{\delta_{\nu,1} + \delta_{\nu,-1}}{2} \Delta J, \quad (47)$$

with integer $\nu_{\ell'\ell} \equiv (w_{\ell'} - w_\ell)/\hbar\omega$ for tunneling from ℓ to ℓ' . Thus, as long as higher harmonics are negligible in the modulated tunneling matrix element $J(t)$, the forcing allows for single-“photon” processes bridging energy differences of $\pm\hbar\omega$.

Such “photon”-assisted tunneling via a modulation of the lattice depth has been observed in Florence (Alberti *et al.*, 2010), where *inter alia* the selectivity to single-“photon” processes has also been used in order to selectively induce and observe tunneling processes between next-nearest and next-next nearest lattice sites. Subsequently, the scheme was employed for a precision measurement of the gravitational acceleration (Poli *et al.*, 2011).

This effect has been combined with strong interactions both with spinless bosons in a tilted lattice by Greiner’s

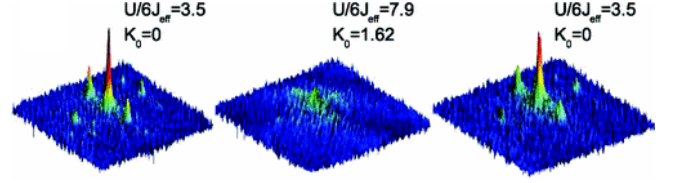


FIG. 2 Dynamically induced Superfluid-to-Mott-insulator transition in a shaken cubic optical lattice. Two-dimensional projection of the momentum distribution obtained from time-of-flight absorption imaging at three different times during the experimental protocol: before ramping up the driving strength $K_0 = K/\hbar\omega$, after K_0 has been ramped up linearly (middle), after K_0 has been ramped down again (right). The loss and re-appearance of sharp peaks indicates that the system approximately followed a many-body Floquet state undergoing a quantum phase transition from a superfluid to a Mott insulator and back. (taken from Zenesini *et al.*, 2009)

group at Harvard (Ma *et al.*, 2011) and with spin-1/2 bosons in a tilted double well by Bloch’s group in Munich (Chen *et al.*, 2011). In these experiments the on-site interaction U is large compared to the tunneling parameter J and comparable to the lattice tilt Δ , so that the resonance condition (38) has to be modified to include also the change of interaction energy associated with a tunneling process. In this way the effective tunneling matrix element becomes occupation dependent. In Greiner’s lab, this effect was employed to measure the Hubbard energy U as well as occupation-number-dependent corrections to it, as they arise from perturbative admixtures of excited Bloch bands. Moreover, it has been used to control (a finite-size precursor of) a phase transition in the effective spin model that the same group had realized already in an earlier experiment with spinless bosons in a tilted lattice (Simon *et al.*, 2011). In the Bloch experiment also second-order tunneling via non-resonant intermediate states was observed at the resonance condition $\hbar\omega = 2\Delta$ and the modulation used to control superexchange processes.

Experiments that use “photon”-assisted tunneling induced by a moving secondary lattice for the purpose of engineering artificial magnetic fields will be reviewed in Sec. III.F.1 below.

D. Dynamic control of the bosonic superfluid-to-Mott-insulator transition

When deriving the approximate effective Hamiltonian (34), in the previous sections it was assumed that the driving frequency is large compared to tunneling and interaction parameters. But it was not required that the interactions are weak compared to the kinetic energy. Therefore, it is possible to control a lattice system also in the strong coupling regime by means of periodic forcing.

This has been exploited in an experiment in Pisa (Zenesini *et al.*, 2009), where the transition between a bosonic superfluid and a Mott-insulator state has been induced by means of lattice shaking. This experiment followed a proposal by Eckardt *et al.*, 2005 (see also Eckardt and Holthaus, 2007).

The bosonic Hubbard model possesses two different ground-state phases, a gapless compressible superfluid phase, with the particles being delocalized, and a gapped incompressible Mott-insulator phase, where an integer number of particles is localized at every lattice site by strong repulsive interactions (Fisher *et al.*, 1989). In a trapped optical lattice system extended Mott-insulator regions form when the ratio between Hubbard interaction and tunneling parameter, U/J , exceeds a critical value (Jaksch *et al.*, 1998), which for the three-dimensional cubic lattice at unit filling is given by $(J/J)_c \approx 29.3$ (Capogrosso-Sansone *et al.*, 2007; Teichmann *et al.*, 2009). This transition has been observed the first time in a seminal experiment with spinless bosons in a cubic optical lattice by Greiner *et al.*, 2002 in Munich, where the ration U/J was increased by ramping up the lattice depth V_0 . As a signature of the transition the experimentalists observed the disappearance of sharp peaks in the momentum distribution, as they characterize the superfluid phase, as well as their reappearance, when the lattice depth was ramped down again.

In the Pisa experiment lattice shaking was employed to lower the effective tunneling parameter (23) with respect to the interaction strength U , which is not altered by the lattice shaking. In order to modify the tunneling matrix element in all three directions of a cubic lattice, the forcing was applied along the diagonal direction. When the shaking amplitude was ramped up smoothly, the sharp momentum peaks characterizing the superfluid ground state disappeared once U/J_{eff} became sufficiently large. The peaks reappeared, when the forcing was ramped down again (see Fig. 2). The interpretation of this experiment is that the system followed approximately a many-body Floquet state that, in response to the variation of the driving amplitude, underwent a transition from a superfluid to a Mott insulator and back. This experiment demonstrates on the one hand that time-periodic forcing is a suitable tool also for the manipulation of strongly interacting many-body systems and their interaction-driven physics. On the other hand, it also is an example of *adiabatic state preparation* in a time-periodically driven system. Such “adiabatic” processes in driven many-body systems will be discussed in more detail in section IV below, where we will point out that they actually correspond to a complex mixture of adiabatic and diabatic processes in an extended Hilbert space.

E. Kinetic frustration

Controlling the spreading of a Bose condensate, Bloch oscillations, or even the superfluid-to-Mott-insulator transition, all these experimentally observed effects discussed above clearly show that periodic forcing is a suitable tool for controlling many-body systems of ultracold atoms in optical lattices. These effects have, however, been achieved also without periodic forcing, e.g. by varying the depth of the optical lattice, leading to an exponential suppression of the tunneling matrix element, or by tuning a Wannier-Stark tilt. But periodic forcing can also be used to engineer systems with qualitatively new properties. One possibility is to effectively modify not only the amplitude, but also the sign or, more generally, the phase of tunneling matrix elements.

In the one-dimensional driven tight-binding chain, with effective dispersion relation $\varepsilon_{\text{eff}}(k_x) = -2J_{\text{eff}} \cos(dk_x)$, a sign change of the effective tunneling matrix element J_{eff} does not lead to qualitatively new physics. The resulting inversion of the dispersion relation can be compensated by a shift in quasimomentum by $\Delta k = \pi/d$, which corresponds to a gauge transformation and leaves also the interactions unchanged. This argument generalizes to other bipartite lattice geometries (like square, hexagonal, or cubic), where a sign change of the tunneling matrix element can be compensated by redefining the sign of the Wannier orbital on every other lattice site. However, for a non-bipartite lattice (like the triangular or the Kagomé lattice), the inversion of the tunneling matrix element does not simply correspond to a gauge transformation, but leads to a geometrically frustrated tunneling kinetics: A negative tunneling parameter $J_{\text{eff}} < 0$, corresponding to a positive tunneling matrix element $-J_{\text{eff}} > 0$, favors the wave function to change sign from one lattice site to the other. Thus, given, e.g., three sites arranged in a triangular plaquette, it is not possible anymore to minimize the kinetic energy at each of the three tunneling bonds at the same time. Especially in combination with strong interactions, such kinetic frustration can give rise to intriguing behavior.

A sign inversion of the effective tunneling parameter can be achieved via periodic forcing (Eckardt *et al.*, 2010). A two-dimensional lattice that is shaken along a circular orbit experiences the inertial force

$$\mathbf{F}(t) = F_\omega [\cos(\omega t) \mathbf{e}_x + \sin(\omega t) \mathbf{e}_y]. \quad (48)$$

In the high-frequency regime its dynamics can be described by the approximate effective Hamiltonian (34) with the isotropic tunneling parameter given by Eq. (23), where $K = dF_\omega$ with lattice constant d . The effective tunneling parameter becomes negative at $K/\hbar\omega \approx 2.4$ and assumes a minimal value of $J_{\text{eff}} \approx -0.4J$ at $K/\hbar\omega \approx 3.8$. On the single-particle level, after an inversion of the tunneling matrix elements, the dispersion

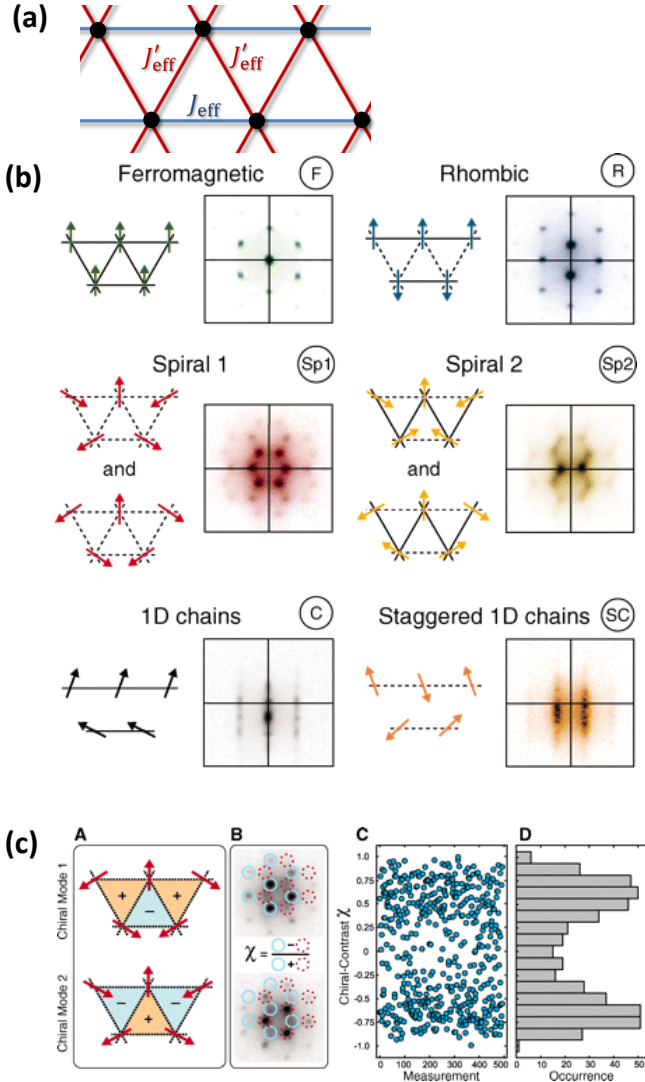


FIG. 3 (a) Anisotropic triangular lattice with effective tunneling parameters J_{eff} and J'_{eff} . (b) Momentum distribution averaged over many measurements (shots) and corresponding pattern of the condensate phase (indicated by direction of arrow) for different J_{eff} and J'_{eff} (dashed/solid lines indicate positive/negative tunneling parameters). (c) Spontaneous time-reversal symmetry breaking for $J_{\text{eff}} = J'_{\text{eff}} < 0$. Each of the two spatial configurations of the condensate phase shown in A breaks time-reversal symmetry. In absorption images the two are distinguished by the position of the measured peaks, indicated by dotted or solid circles in B. The contrast between both configurations χ varies from shot to shot (C) giving a bimodal distribution (D), so that typically only one of the two configurations appears spontaneously. [(b) and (c) taken from Struck *et al.*, 2011]

relation of the triangular lattice $\varepsilon_{\text{eff}}(\mathbf{k})$ possesses two inequivalent minima $\mathbf{k} = \pm \mathbf{q}$. For a Bloch wave function $\psi_{\ell} = M^{-1/2} \exp(i\varphi_{\ell})$ with $\varphi_{\ell} = \mathbf{k} \cdot \mathbf{r}_{\ell}$ on the lattice, where M denotes the total number of lattice sites, the

effective kinetic energy is given by

$$\varepsilon_{\text{eff}}(\mathbf{k}) = -\frac{J_{\text{eff}}}{M} \sum_{\langle \ell' \ell \rangle} \cos(\varphi_{\ell'} - \varphi_{\ell}) = -J_{\text{eff}} \sum_{\mathbf{d}} \cos(\mathbf{d} \cdot \mathbf{k}), \quad (49)$$

where the second sum runs over the six vectors \mathbf{d} that connect each lattice site with its nearest neighbors. The phases φ_{ℓ} play the role of coupled classical rotors. For antiferromagnetic coupling, $J_{\text{eff}} < 0$, this energy becomes minimal for the two spiral phase patterns denoted “Spiral 1” in Fig. 3(b), characterized by $\mathbf{k} = \pm \mathbf{q}$ with $\mathbf{q} = (q_x, 0, 0)$ and $q_x = 4\pi/(3d)$.

Considering many, weakly repulsive, spinless bosons, the ground state of the effective Hamiltonian corresponds to a Bose condensate in one of the two minima of the effective dispersion relation [states involving both quasi-momenta \mathbf{q} and $-\mathbf{q}$, either in a coherent superposition or by forming a fragmented condensate, are disfavored by repulsive interactions (Eckardt *et al.*, 2010)]. This form of spontaneous time-reversal symmetry breaking has been observed in a system of weakly interacting spinless bosons in a triangular lattice of one-dimensional tubes in Sengstock’s group in Hamburg (Struck *et al.*, 2011), see Fig. 3(c).

Extending the scheme to elliptical forcing causes an anisotropic modification of tunneling, since the amplitude of the forcing K acquires a directional dependence. In a triangular lattice this allows for creating the pattern of tunneling matrix elements depicted in Fig. 3(a). The parameter space spanned by J_{eff} and J'_{eff} has been explored in the Hamburg experiment. Fig. 3(b) shows the measured momentum distributions, which feature peaks at the expected positions corresponding to the sketched phase patterns. The degree of kinetic frustration is basically controlled by $J_{\text{eff}}/|J'_{\text{eff}}|$. For $J_{\text{eff}} = 0$, the remaining J'_{eff} bonds form a bipartite rhombic lattice, which does not feature frustration and favors a staggered Néel-type order of the phases φ_{ℓ} [denoted “rhombic” in Fig. 3(b)] for antiferromagnetic coupling $J'_{\text{eff}} < 0$. Switching on a finite antiferromagnetic $J_{\text{eff}} = -\gamma|J'_{\text{eff}}| < 0$ leads to frustration for either sign of J'_{eff} , and causes spontaneous time-reversal symmetry breaking when $\gamma > \gamma_c$. The corresponding phase patterns are denoted by “Spiral 1” and “Spiral 2” for $J'_{\text{eff}} < 0$ and $J'_{\text{eff}} > 0$, respectively. The critical parameter is roughly given by $\gamma_c \approx 0.5$, where the single-particle dispersion relation develops two minima, though interaction-induced quantum fluctuations are expected to shift it to slightly larger values (Eckardt *et al.*, 2010).

The idea of achieving kinetic frustration via lattice shaking is of interest mainly for bosons. For fermions, an inversion of tunneling matrix elements results already from a particle-hole transformation, so that kinetic frustration will naturally appear when the Fermi energy becomes sufficiently large. Apart from the triangular lattice, the scheme can be used to induce kinetic frustra-

tion also in other non-bipartite lattice geometries. For an optical Kagomé lattice, as it has been realized experimentally recently (Jo *et al.*, 2012), the impact of kinetic frustration would be even more drastic. After inverting the sign of the tunneling parameters the lowest of the three bands will be completely flat, so that even weak interactions will have a major impact on the ground state (Huber and Altman, 2010). Also one-dimensional chains, like the saw-tooth (Huber and Altman, 2010) or zig-zag (Greschner *et al.*, 2013) lattice, can acquire kinetic frustration in response to lattice shaking as well as non-bipartite three-dimensional lattice geometries, such as pyrochlore. Kinetic frustration enhances the role of interactions not only in the extreme case of lattice geometries acquiring a flat lowest band. In the triangular lattice the critical interaction strength for the formation of a Mott-insulator will be reduced (Eckardt *et al.*, 2010) and it can even become zero in the zig-zag chain (Greschner *et al.*, 2013). Note that the system can form a chiral Mott insulator, with spontaneously broken time-reversal symmetry breaking appearing in the particle-hole fluctuations (Greschner *et al.*, 2013; Zaletel *et al.*, 2014).

It is also an interesting perspective to explore the interplay of kinetic frustration with very strong interactions. In the limit of hard-core bosons the effective Hamiltonian (34) can be mapped to a quantum spin-1/2 *XY* model (Eckardt *et al.*, 2010)

$$\hat{H}_{\text{eff}} = -J_{\text{eff}} \sum_{\langle \ell' \ell \rangle} \hat{S}_{\ell'}^+ \hat{S}_{\ell}^- = -J_{\text{eff}} \sum_{\langle \ell' \ell \rangle} \left(\hat{S}_{\ell'}^x \hat{S}_{\ell}^x + \hat{S}_{\ell'}^y \hat{S}_{\ell}^y \right). \quad (50)$$

Here the \hat{S}_{ℓ} denote standard spin operators acting on the pseudo-spin degree of freedom spanned by the two states “there is a boson” (\uparrow) and “there is no boson” (\downarrow). In the experiment mentioned above, reaching this regime would require a further confinement perpendicular to the lattice, making the system effectively two-dimensional. For non-bipartite lattices and $J_{\text{eff}} < 0$ the Hamiltonian (50) describes frustrated quantum antiferromagnetism. The ground-state (and low-temperature) regime of such frustrated quantum magnets can give rise to intriguing physics, like the formation of topological or critical spin liquids. However, the theoretical prediction of the nature of the ground state is typically a hard problem (Balents, 2010; Moessner and Ramirez, 2006; Sachdev, 2008). Possibly, future experiments simulating the Hamiltonian (50) in shaken optical lattices of various geometries could provide useful information concerning this issue. Here a promising feature is that the model (50) is based on easy-to-cool motional bosonic degrees of freedom, with the coupling on the order of the tunneling matrix element $J_{\text{eff}} \sim J$. Without a lattice, bosonic systems have been cooled down to entropies per particle as low as $0.001k_B$ (Olf *et al.*, 2015). This contrasts with optical-lattice spin systems based on a Mott insulator of spin-1/2 fermions, with small superexchange cou-

pling $\sim J^2/U \ll J$ between neighboring spins. For spin-1/2 fermions entropies per particle of about $0.6k_B$ in the Mott-insulating state (Boll *et al.*, 2016; Greif *et al.*, 2013; Hart *et al.*, 2015) and $0.04k_B$ in a system without lattice (Ku *et al.*, 2012) have been achieved. Moreover, close analogies between ground and low-energy states of frustrated *XY* and Heisenberg antiferromagnets might permit to shed light also on the physics of the latter (Läuchli and Moessner, 2015).

F. Artificial magnetic fields – High-frequency schemes

Inverting the sign of the tunneling matrix elements can be viewed as a special case of a more general scheme where the effective matrix element for tunneling from ℓ to ℓ' acquires a *phase*,

$$J_{\ell'\ell}^{\text{eff}} = |J_{\ell'\ell}^{\text{eff}}| e^{i\theta_{\ell'\ell}^{\text{eff}}}. \quad (51)$$

Such effective Peierls phases $\theta_{\ell'\ell}^{\text{eff}}$ play the role of a vector potential. The tight-binding representation of a vector potential $\mathbf{A}(\mathbf{r})$ is, according to the Peierls substitution, given by $\theta_{\ell'\ell} = \frac{1}{\hbar} \int_{\mathbf{r}_{\ell}}^{\mathbf{r}_{\ell'}} d\mathbf{r} \cdot \mathbf{A}(\mathbf{r})$, where we have absorbed the charge in the definition of \mathbf{A} so that it carries the dimension of a momentum and where the integration is taken along a straight line. In the last years, such effective Peierls phases have been realized by means of periodic forcing in several experiments (Aidelsburger *et al.*, 2013, 2011, 2015; Atala *et al.*, 2014; Kennedy *et al.*, 2015; Miyake *et al.*, 2013; Struck *et al.*, 2012, 2013).

Of particular interest is the situation where the Peierls phases describe a finite effective magnetic flux Φ_P^{eff} through a lattice plaquette P . It is defined as the dimensionless Aharonov-Bohm-like phase $\Phi_P^{\text{eff}} = \sum_P \theta_{\ell'\ell}^{\text{eff}}$ obtained by summing over the Peierls phases picked up when tunneling once around the plaquette in positive direction, as depicted in Fig. 4. The plaquette flux is defined modulo the dimensionless magnetic flux quantum of 2π only, it is gauge invariant and plays the role of the magnetic field (flux density) in continuous systems. The creation of effective plaquette fluxes by means of periodic forcing turned out to be a powerful method for the creation of *artificial* (or *synthetic*) magnetic fields for charge-neutral particles in optical lattices (other schemes rely on laser-dressing of internal atomic degrees of freedom, Dalibard *et al.*, 2011 and Goldman *et al.*, 2014). In this way extremely strong fields of the order of the maximum possible flux of π can be achieved. To put this in perspective, for an electron a flux of π through the hexagonal plaquette of graphene with area $A_{\text{hex}} \approx 5.2\text{\AA}^2$ would correspond to the enormous magnetic field strength $B = \pi\hbar/(eA_{\text{hex}}) \approx 3.9 \cdot 10^4\text{T}$, which is more than two orders of magnitude larger than the real magnetic fields that can be achieved in the laboratory.

The experiments to be discussed in the following are

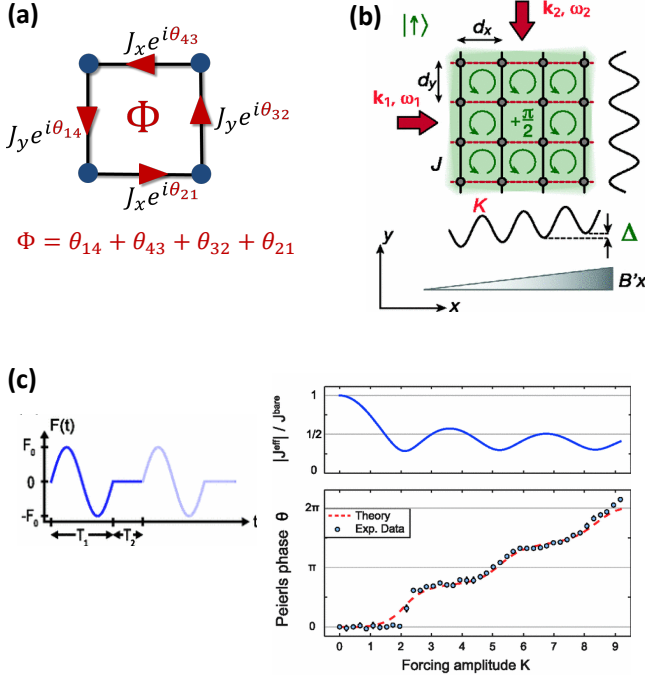


FIG. 4 (a) The dimensionless magnetic flux Φ piercing a lattice plaquette equals the sum of the Peierls phases $\theta_{\ell'\ell}$ picked up when moving around it in positive direction. (b) Moving-secondary-lattice scheme for creating a homogeneous flux configuration. (d) Asymmetric lattice shaking (left) gives rise to complex effective tunneling matrix elements (right), plotted versus $K = F_0 d T_1 / T$ (in units of $\hbar\omega$) for $T_1/T_2 = 2.1$. [taken from: (b) Aidelsburger *et al.*, 2011, (c) from Aidelsburger *et al.*, 2013, (d) Struck *et al.*, 2012]

based on tailoring on-site potentials of the form

$$w_\ell(t) = w_\ell^{\text{dr}}(t) + \nu_\ell \hbar\omega, \quad (52)$$

appearing in the Hamiltonian (24), with time-periodic potential modulation $w_\ell^{\text{dr}}(t) = w_\ell^{\text{dr}}(t+T)$ of zero average, $\frac{1}{T} \int_0^T dt w_\ell^{\text{dr}}(t) = 0$, and possibly also a static part with integers ν_ℓ . In the high-frequency regime, a system that is driven like that will again be described by an effective Hamiltonian of the form (34), with the tunneling matrix elements $J_{\ell'\ell}^{\text{eff}}$ given by Eq. (35) depending on $w_\ell(t)$ as specified by Eq. (27).

Before reviewing specific schemes and experiments, let us identify necessary conditions for the creation of artificial gauge fields (Hauke *et al.*, 2012, a general discussion of symmetries of the effective Hamiltonian is furthermore given by Kitagawa *et al.*, 2010). For that purpose, we choose the gauge constant $\chi_{0\ell}$ in Eq. (27) such that $\chi_\ell(t) = \chi_\ell^{\text{dr}}(t) - \nu_\ell \omega t + \gamma_\ell$, with $\chi_\ell^{\text{dr}}(t)$ having zero average, $\frac{1}{T} \int_0^T dt \chi_\ell^{\text{dr}}(t) = 0$, and with yet undetermined constants γ_ℓ representing the gauge freedom. The imaginary part of the effective tunneling matrix element $J_{\ell'\ell}^{\text{eff}}$ is given by $I_{\ell'\ell} = -\frac{J}{T} \int_0^T dt \sin(\chi_\ell^{\text{dr}}(t) - \nu_{\ell'\ell} \omega t + \gamma_\ell - \gamma_{\ell'})$, where $\chi_{\ell'\ell}^{\text{dr}} = \chi_{\ell'}^{\text{dr}} - \chi_\ell^{\text{dr}}$ and $\nu_{\ell'\ell} = \nu_{\ell'} - \nu_\ell$. If one can find gauge

constants γ_ℓ such that all $I_{\ell'\ell}$ vanish, one cannot create plaquette fluxes $\Phi_P^{\text{eff}} \neq 0, \pi$ that break time reversal symmetry (where the special case $\Phi_P^{\text{eff}} = \pi$ corresponds to the situation of kinetic frustration discussed above).

Let us first discuss the case, where the static potential off-sets vanish, $\nu_{\ell'\ell} = 0$. One can identify two temporal symmetries of the relative potential modulations $w_{\ell'\ell}^{\text{dr}} \equiv w_{\ell'}^{\text{dr}} - w_\ell^{\text{dr}}$ that imply $I_{\ell'\ell} = 0$ for the choice $\gamma_\ell = \gamma_{\ell'} = 0$. These are the *local reflection symmetry*

$$w_{\ell'\ell}^{\text{dr}}(t - \tau_{\ell'\ell}) = w_{\ell'\ell}^{\text{dr}}(-t - \tau_{\ell'\ell}) \quad \forall \langle \ell' \ell \rangle \quad (53)$$

with respect to times $\tau_{\ell'\ell}$ defined individually on each local bond $\langle \ell' \ell \rangle$, and the *shift symmetry*

$$w_{\ell'\ell}^{\text{dr}}(t) = -w_{\ell'\ell}^{\text{dr}}(t - T/2) \quad \forall \langle \ell' \ell \rangle. \quad (54)$$

Either of these symmetries implies that the effective Hamiltonian preserves time-reversal symmetry. Note that precisely these symmetries are also known to prevent ratchet-type transport (Denisov *et al.*, 2007; Flach *et al.*, 2000).⁷ A sinusoidal potential modulation obeys both symmetries.

If additional to the potential modulations also finite potential off-sets $\nu_{\ell'\ell} \neq 0$ are created, so that the driving has to induce “photon” assisted tunneling, the above symmetries are not enough to enforce time-reversal symmetry $I_{\ell'\ell} = 0$. Instead this can be achieved by choosing $\gamma_\ell = -\nu_\ell \omega \tau$, if the *global reflection symmetry*

$$w_{\ell'\ell}^{\text{dr}}(t - \tau) = w_{\ell'\ell}^{\text{dr}}(-t - \tau) \quad \forall \langle \ell' \ell \rangle \quad (55)$$

is fulfilled with respect to a globally defined time τ .

Involving “photon” assisted tunneling against non-zero potential off-sets $\nu_{\ell'\ell} \hbar\omega$ poses less constraints for the creation of artificial gauge fields, since only the global reflection symmetry (55) has to be broken. As a consequence, already sinusoidal forcing

$$w_\ell^{\text{dr}}(t) = K \sin(\omega t - \varphi_\ell) \quad (56)$$

can produce plaquette fluxes $\Phi_P^{\text{eff}} \neq 0, \pi$, provided the driving phase φ_ℓ varies from site to site. This has been proposed theoretically (Bermudez *et al.*, 2011; Kolovsky, 2011) and demonstrated in a series of beautiful experiments in the groups of Bloch in Munich (Aidelsburger *et al.*, 2013, 2011, 2015; Atala *et al.*, 2014) and Ketterle at MIT (Kennedy *et al.*, 2015; Miyake *et al.*, 2013). For $\gamma_\ell = 0$, one finds

$$J_{\ell'\ell}^{\text{eff}} = J \mathcal{J}_{\nu_{\ell'\ell}} \left(\frac{K_{\ell'\ell}}{\hbar\omega} \right) e^{i\nu_{\ell'\ell} \varphi_{\ell'\ell}}, \quad (57)$$

with amplitude $K_{\ell'\ell} = 2K \sin(\varphi_{\ell'} - \varphi_\ell)$ and phase $\varphi_{\ell'\ell} = (\varphi_{\ell'} + \varphi_\ell)/2$ of the relative potential modulation $w_{\ell'\ell}^{\text{dr}}(t)$.

⁷ Such directed transport has also been studied experimentally with atomic quantum gases in driven optical lattices in Weitz’s group in Bonn (Salger *et al.*, 2013, 2009).

1. Moving-secondary-lattice scheme

Experimentally a site-dependent driving phase φ_ℓ has been achieved by combining two slightly detuned laser waves $\propto \exp(i\mathbf{k}_{1,2} \cdot \mathbf{r} - \omega_{1,2}t)$, which create a shallow secondary lattice of depth $2K$ that moves with respect to the deep host lattice.⁸ This moving secondary lattice causes sinusoidal potential modulations $w_\ell^{\text{dr}}(t)$ of frequency $\omega = (\omega_1 - \omega_2)/2$ and spatially dependent driving phase $\varphi_\ell = \mathbf{q} \cdot \mathbf{r}_\ell$ with $\mathbf{q} = (\mathbf{k}_1 - \mathbf{k}_2)/2$. A configuration of particular interest is shown in Fig. 4(b). For a square lattice $\mathbf{q} = (q_x, q_y)$ is combined with a strong static potential gradient in one of the lattice directions, $\nu_\ell = x_\ell/d$ (Aidelsburger *et al.*, 2013; Miyake *et al.*, 2013). The resulting effective parameters for tunneling in x and y direction read

$$J_x^{\text{eff}} = J_x \mathcal{J}_1\left(\frac{K_x}{\hbar\omega}\right) e^{i\mathbf{q} \cdot (\mathbf{r}_{\ell'} + \mathbf{r}_\ell)/2}, \quad J_y^{\text{eff}} = J_y \mathcal{J}_0\left(\frac{K_y}{\hbar\omega}\right), \quad (58)$$

with $K_i = 2 \sin(d_i q_i) K$, where d_i and J_i denote the lattice spacing and the tunneling parameter in both directions $i = x, y$, respectively.

The y -dependent part $q_y y$ of the Peierls phase for “photon” assisted tunneling in x direction, gives rise to an effective flux of

$$\Phi_{\text{eff}} = dq_y, \quad (59)$$

piercing every lattice plaquette. The effective Hamiltonian describes particles on a square lattice subjected to a homogeneous magnetic field and corresponds to the paradigmatic Harper Hamiltonian (Harper, 1955). It is famous for the fractal structure of its single-particle spectrum plotted versus $\alpha = \Phi_{\text{eff}}/2\pi$, the Hofstadter butterfly (Hofstadter, 1976). It results from the possibility that the area $d_x d_y / \alpha$ of the magnetic unit cell can become an incommensurate multiple of the area $d_x d_y$ of the square-lattice unit cell. If the potential gradient results from a Zeeman field the sign of the magnetic flux will depend on the spin state of the atoms (Aidelsburger *et al.*, 2013; Kennedy *et al.*, 2013; Miyake *et al.*, 2013). If the potential gradient is replaced by an optical superlattice, so that $\nu_\ell = [1 + (-1)^{x_\ell/d}]/2$ gives rise to staggered potential off-sets $\nu_{\ell'} \hbar\omega$, and a staggered pattern of fluxes $\pm |\Phi_{\text{eff}}|$ (Aidelsburger *et al.*, 2011). In order to realize the Harper Hamiltonian also for the superlattice configuration, the flux can be rectified by combining two moving secondary lattices such that driving phases $\varphi_{\ell'\ell}$ are obtained that compensate the staggered potential offsets (Aidelsburger *et al.*, 2015).

Experimentalists have investigated the ground state of a weakly interacting Bose gas in effective lattice models created using the moving-secondary-lattice scheme. Their observations reflect the fact that finite plaquette fluxes introduce frustration into the tunneling kinetics. This frustration results from the fact that the phase-winding of the wave function around the plaquette has to be an integer multiple of 2π , while the optimal phase differences at the tunneling bonds, which are given by $\theta_{\ell'\ell}^{\text{eff}}$, sum up to Φ_{eff} . The frustration becomes maximum for the maximum phase mismatch $\Phi_{\text{eff}} \bmod 2\pi = \pi$. For a fixed flux the degree of frustration can be controlled by the relative strength of different tunneling parameters, since it becomes energetically less costly to accommodate a greater share of the phase mismatch at weaker tunneling links. In the experiment by Aidelsburger *et al.*, 2011 the bosonic ground state for a staggered flux configuration with $\Phi_{\text{eff}} = \pm\pi/2$ was explored. The unit cell contains two sites, giving rise to two bands. If the ratio $\gamma = |J_x^{\text{eff}}|/|J_y^{\text{eff}}|$ becomes larger than the critical values of $\gamma_c = \sqrt{2}$, the central minimum of the lowest band splits continuously into two minima that separate in k_y -direction. That is, while for $\gamma \leq \gamma_c$ the wave function does not adapt its momentum to the plaquette flux, for larger γ a two-fold degenerate spiral phase pattern around the lattice plaquettes becomes more favorable. This resembles the case of the frustrated triangular lattice reviewed in the previous section. However, different from the triangular lattice, a homogeneous density distribution, as it is favored by the repulsive interactions, is achieved by a coherent superposition of both ground states (Möller and Cooper, 2010), which has been observed in the experiment.

Reducing the geometry to one-dimensional ladders with constant plaquette flux $\pi/2$ by suppressing tunneling at every other link in x direction for the model of Fig. 4(b), the transition at $\gamma = \gamma_c$ finds an appealing interpretation as an analog of the Meissner effect in superconductors (Orignac and Giamarchi, 2001). For $\gamma < \gamma_c$, corresponding to the phase of low magnetic fields, the wave function is stiff, so that the Peierls phases cause a circular Meissner current around the whole ladder. In turn, when $\gamma > \gamma_c$, the wave function adapts to the field, corresponding to the formation of vortices. This effect was observed by Atala *et al.*, 2014.

Very recently, the bosonic superfluid ground state, or more precisely a low-entropy state close to it, was prepared using the tilted-lattice configuration giving rise to a plaquette of π [as depicted in Fig. 4(b), but with $\Phi_{\text{eff}} = \pi$ (Kennedy *et al.*, 2015)]. Even in the presence of a rather deep lattice (of more than ten recoil energies) in the perpendicular z direction, which leads to a significant increase of interactions and which can be used to reduce the dynamics to two dimensions, rather large coherence times were observed. This is a promising step towards the preparation of strongly correlated fractional

⁸ This configuration resembles the one employed in an earlier proposal for the creation of artificial magnetic fields by Jaksch and Zoller, 2003, which is based on Raman transitions between internal atomic states.

quantum-Hall-type states in optical lattices with artificial magnetic fields.

Also dynamical signatures of artificial magnetic fields have been probed experimentally. Conceptually maybe the most straightforward signature is the observation of the cyclotron-type dynamics of a single particle on an isolated plaquette of the square lattice (Aidelsburger *et al.*, 2013, 2011). An intriguing effect is, moreover, the observation of a quantized Hall velocity with *thermal bosons* in a square lattice with homogenous flux (Aidelsburger *et al.*, 2015). For a quarter of a flux quantum per plaquette the elementary lattice cell is enlarged to the area $A_m = 4d^2$ of four plaquettes pierced by one flux quantum and the Hubbard model describes four Bloch bands. The lowest band has favorable properties. It is rather flat, i.e. it is separated by a large energy gap of about seven times the band width, and characterized by a Chern number $C_0 = 1$. For the b th band of a two-dimensional lattice this topological index is defined like

$$C_b = \frac{1}{2\pi} \int_{\text{BZ}} dk_x dk_y \Omega_b(\mathbf{k}), \quad (60)$$

where the integral is taken over the reduced first Brillouin zone of area $(2\pi)^2/A_m$ corresponding to the enlarged lattice cell A_m . Moreover, $\Omega_b(\mathbf{k})$ denotes the Berry curvature with respect to quasimomentum \mathbf{k} . It is given by $\Omega_b(\mathbf{k}) = \mathbf{e}_z \cdot \boldsymbol{\Omega}_b(\mathbf{k})$ with $\boldsymbol{\Omega}_b(\mathbf{k}) = \nabla_{\mathbf{k}} \times \mathbf{A}_b(\mathbf{k})$ and Berry connection $\mathbf{A}_b(\mathbf{k}) = i\langle u_b(\mathbf{k}) | \nabla_{\mathbf{k}} | u_b(\mathbf{k}) \rangle$. Here $|u_b(\mathbf{k})\rangle$ is the spatially periodic part of the Bloch state with quasimomentum \mathbf{k} of band b . The Chern number is quantized and can take integer values only. This is a consequence of the fact that it corresponds to $(2\pi)^{-1}$ times the Berry phase associated with a closed surface in quasimomentum space, namely the torus given by the first-Brillouin zone. In the presence of a homogeneous force \mathbf{F} the velocity associated with a Bloch state is given by (see, e.g. Xiao *et al.*, 2010)

$$\mathbf{v}_b(\mathbf{k}) = \frac{1}{\hbar} [\nabla_{\mathbf{k}} \varepsilon_b(\mathbf{k}) - \mathbf{F} \times \boldsymbol{\Omega}_b(\mathbf{k})]. \quad (61)$$

The “anomalous” second term describes a Hall drift (Karplus and Luttinger, 1954). For a homogeneously filled band, the mean velocity of the particles is given by

$$\bar{\mathbf{v}}(\mathbf{k}) = \frac{A_m}{(2\pi)^2} \int_{\text{BZ}} dk_x dk_y \mathbf{v}_b(\mathbf{k}) = -A_m \frac{C_b}{\hbar} \mathbf{e}_z \times \mathbf{F}, \quad (62)$$

where we have used Eq. (61) and the fact that the first term on the left-hand-side of Eq. (61) averages to zero. The velocity is proportional to the Chern number C_b and, therefore, quantized. For a fermionic band insulator, with the B lowest bands filled completely, this result implies a quantized Hall conductivity $\sigma_h = C/\hbar$ with $C = \sum_{b \leq B} C_b$ (Thouless *et al.*, 1982).⁹ For $C \neq 0$

this is the integer quantum Hall effect and the system is a topological insulator called Chern insulator (Hasan and Kane, 2010; Qi and Zhang, 2011). However, in the experiment by Aidelsburger *et al.*, 2015, the flatness of the lowest band is exploited in order to create a thermal state, where weakly interacting bosons occupy (to good approximation) the lowest band in a uniform fashion, but no excited bands. Extracting the Hall displacement of the cloud in response to a force \mathbf{F} the Chern number C_0 was measured to be 0.99(5) in excellent agreement with theory. Here an effective force $F_x = \delta/d$ results from a slight detuning δ between the driving frequency and the potential off set between neighboring sites to be overcome by “photon”-assisted tunneling [Eq. (38)]. Also the breakdown of the Hall response was observed at a topological transition to a lattice structure with $C_0 = 0$ induced by a superlattice potential was observed.

2. Asymmetric-lattice-shaking scheme

A different scheme for the creation of artificial magnetic fields does not require potentials off-sets with finite $\nu_{\ell'\ell}$, and can be realized by means of lattice shaking (Hauke *et al.*, 2012; Struck *et al.*, 2012, 2013). It is based on breaking both the local reflection symmetry (53) and the shift symmetry (54) by employing non-sinusoidal driving functions $w_{\ell}^{\text{dr}}(t)$. The fact that the optical-lattice physics happens at rather low energy scales, so that the driving frequencies $\omega/2\pi$ required for the high-frequency approximation (34) and (35) are in the lower kilohertz regime, allows for the implementation of practically arbitrary shaking functions. In a first experiment, a one-dimensional lattice has been subjected to the inertial force depicted in Fig. 4(c), which led to the complex tunneling parameter $J_{\text{eff}} = |J_{\text{eff}}|e^{i\theta_{\text{eff}}}$ shown in the same figure. While in a one-dimensional chain no magnetic field is created by a finite Peierls phase, its impact, a shift of the effective dispersion relation $\varepsilon_{\text{eff}}(k_x)$ by θ_{eff}/d , can still be observed. When θ_{eff} (representing the x component of a homogeneous, but time-dependent vector potential) is rapidly ramped up this creates a significant conservative force (the shifted dispersion relation possesses a finite group velocity at the initial condensate momentum $k_x = 0$). This initiates an oscillatory dynamics in the trap. When θ_{eff} is switched on slowly the trapped condensate follows the minimum of the dispersion relation. This gives rise to a peak shift by $k_{\text{shift}} = \theta_{\text{eff}}/d$ in the measured momentum distribution (see discussion in the last paragraph of section III.B), from which the Peierls phase θ_{eff} was inferred (data points in Fig. 4(c)).

Asymmetric lattice shaking can be employed to realize effective magnetic fluxes through such lattice plaquettes that do not feature pairwise parallel edges (whose contribution to the flux would mutually cancel). This has been used in an experiment by Struck *et al.*, 2013 to cre-

⁹ $\sigma_h = Ce^2/\hbar$ for charged particles with elementary charge e .

ate a staggered flux configuration in a triangular lattice (of one-dimensional tubes), with fluxes

$$\Phi_{\Delta}^{\text{eff}} = \Phi_{\text{eff}} \quad \text{and} \quad \Phi_{\nabla}^{\text{eff}} = -\Phi_{\text{eff}} \quad (63)$$

for the two types of plaquette orientations. Unless $\Phi_{\text{eff}} = 0$ or π , these fluxes break time-reversal symmetry in the approximate effective Hamiltonian (34). But they do not break the translational symmetry of the lattice so that the tight-binding model still gives rise to a single band. This is different compared to the square lattice with homogeneous flux [Fig. ??(b)] realized using the moving-secondary-lattice scheme, where an enlarged magnetic unit cell leads to the formation of several bands. Another difference between both schemes concerns the limit of small driving amplitudes $K/\hbar\omega$: for the moving-secondary-lattice-assisted tunneling against a finite off-set $\nu_{\ell'\ell}\hbar\omega$ the amplitude of the tunneling matrix element vanishes and the Peierls phase remains constant [like for J_x^{eff} in Eq. (58)], whereas for the asymmetric driving scheme with $\nu_{\ell'\ell} = 0$ the amplitude remains finite and the Peierls phase continuously approaches zero [as shown in Fig. 4(c)].

The possibility of the asymmetric driving scheme to continuously tune Peierls phases and plaquette fluxes *in situ* has been employed in the triangular lattice experiment in order to tune the system away from the π -flux configuration resulting from the sign-change of the tunneling parameter discussed in the previous section III.E. Realizing

$$\Phi_{\text{eff}} = \pi + \delta, \quad (64)$$

a small δ favors one of the two symmetry broken ground states of the weakly interacting Bose gas [Fig. 3(c)], so that δ controls a first-order phase transition at $\delta_c = 0$. As a signature of the discontinuous nature of the transition the disfavored state remains metastable in the vicinity of the transition (potentially causing hysteresis). This was inferred from the observation that the distribution shown in Fig. 3(c) becomes asymmetric for finite δ , but remains bimodal up to $|\delta| \approx 0.1\pi$ (Struck *et al.*, 2013). It has, moreover, been observed that the time-reversal symmetry breaking and the metastable state vanish for large temperatures. The interesting question whether time-reversal symmetry breaking disappears together with Bose condensation or in a separate transition at a higher temperature could not be resolved.

3. Further possibilities

Apart from the moving-secondary-lattice scheme and the asymmetric-lattice-shaking scheme, there are also proposals for the dynamic creation of artificial magnetic fluxes that are based on a joint modulation of both on-site energies and tunneling parameters (Lim

et al., 2008; Sørensen *et al.*, 2005). Moreover, extensions of the moving-secondary-lattice and the asymmetric shaking schemes have been proposed for the creation of Haldane-type hexagonal-lattice Chern insulators, non-abelian gauge fields (spin-orbit coupling) and topological (spin-Hall) insulators, as well as Weyl semi-metals (Baur *et al.*, 2014; Dubček *et al.*, 2014; Kennedy *et al.*, 2013; Struck *et al.*, 2012). Moreover, another approach for Floquet engineering of artificial magnetic fields or spin-orbit coupling is to construct driving protocols given by a sequence of pulses during which different external fields are present (Goldman and Dalibard, 2014). This includes, moreover, proposals for the creation of spin-orbit coupling in continuous (non-lattice) systems of ultracold atoms using a sequence of magnetic field pulses (Anderson *et al.*, 2013; Xu *et al.*, 2013) as well as for the realization of Floquet topological Chern insulators using pulsed tunneling matrix elements in lattice systems (Kitagawa *et al.*, 2011; Rudner *et al.*, 2013). A discussion of Floquet-topological insulators, which are based on intermediate driving frequencies, will be given in section III.H. Section IV.D is, moreover, devoted to anomalous topological edge states and the bulk-boundary correspondence in periodically driven lattice systems.

It is an interesting perspective to combine both schemes discussed in this section with strong interactions. The flat topological band of the $\pi/2$ Harper model realized by Aidelsburger *et al.*, 2015 together with the promising creation of low-entropy states in such a system (Kennedy *et al.*, 2015) make this system a candidate for the stabilization of topologically ordered fractional-quantum-Hall-type states (fractional Chern insulators, Bergholtz and Liu, 2013 and Parameswaran *et al.*, 2013). Moreover, in the hard-core boson limit, the time-reversal symmetry breaking, as it can be induced by asymmetrically shaking the triangular lattice, introduces Dzyaloshinskii-Moriya interactions $\mathbf{D} \cdot (\hat{\mathbf{S}}_{\ell'} \times \hat{\mathbf{S}}_{\ell})$ to the effective spin model (50), extending the tool box for quantum engineering of spin Hamiltonians. Namely, for hard-core bosons the tunneling term $-(J_{\text{eff}} \hat{a}_{\ell'}^{\dagger} \hat{a}_{\ell} + \text{h.c.})$ with complex $-J_{\text{eff}} = R + iI$ corresponds to

$$2R(\hat{S}_{\ell'}^x \hat{S}_{\ell}^x + \hat{S}_{\ell'}^y \hat{S}_{\ell}^y) + 2I\mathbf{e}_z \cdot (\hat{\mathbf{S}}_{\ell'} \times \hat{\mathbf{S}}_{\ell}) \quad (65)$$

in the language of spin-1/2 operators.

G. Coherent resonant band coupling

Periodic driving can not only bridge large energy offsets between neighboring sites, but it can also induce coherent resonant coupling to excited Bloch bands. This possibility has been explored experimentally in Chu's group in Stanford (Gemelke *et al.*, 2005), in Greiner's group at Harvard (Bakr *et al.*, 2011), and in Chin's group in Chicago (Ha *et al.*, 2015; Parker *et al.*, 2013).

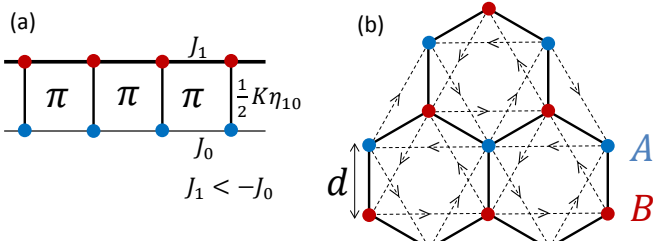


FIG. 5 (a) By resonantly coupling the two lowest bands of a cosine lattice a frustrated ladder is created with plaquette fluxes of π . (b) Hexagonal lattice. The effective Hamiltonian of the driven system including next-nearest-neighbor tunneling with Peierls phase θ (along the dashed lines).

In the Stanford and Chicago experiments, conducted with weakly interacting bosons, the lowest two bands of a cosine lattice have been coupled by means of lattice shaking with the driving frequency $\hbar\omega$ bridging the gap between both bands. Assuming that the coupling to even higher-lying bands is off-resonant and negligible, in this way an effective hybridized band structure is created. The coupling between both bands happens predominantly on-site. Introducing the label $\alpha = 0, 1, \dots$ for the Bloch bands and their Wannier orbitals with respect to one lattice direction, x , an inertial force (22) oriented in this direction gives rise to oscillating coupling matrix elements $K\eta_{\alpha'\alpha}\cos(\omega t)\hat{a}_{\alpha'\ell}^\dagger\hat{a}_{\alpha\ell}$. Here the dimensionless dipole matrix element $\eta_{\alpha'\alpha}$ vanishes for Wannier states of the same parity, i.e. when $(\alpha' - \alpha)$ is even. Analogously to the case of photon-assisted tunneling (47) via a modulation of the tunneling matrix element (44), one finds an effective description where the $\alpha = 1$ Wannier states have the shifted energy $\epsilon_1 - \hbar\omega$ and couple to the $\alpha = 0$ states via effective matrix element $K\eta_{10}/2$. The band-coupled system can be viewed as a ladder, with the Wannier states of each band forming one leg [Fig. 5(a)]. The tunneling parameters J_α of both bands differ in sign and magnitude, $J_1 < -J_0$, so that the ladder is frustrated by plaquette fluxes of π (Sträter and Eckardt, 2015). The effective band structure results from hybridization of the effective dispersion relations of both bands, $\varepsilon_0^{\text{eff}}(k_x) = -J_0\mathcal{J}_0(K/\hbar\omega)\cos(dk_x)$ and $\varepsilon_1^{\text{eff}}(k_x) = \epsilon_1 - \hbar\omega + J_1\mathcal{J}_0(K/\hbar\omega)\cos(dk_x)$, where ϵ_1 is the band-center energy of the first excited band (Drese and Holthaus, 1996).

In the experiment by Gemelke *et al.*, 2005, $\varepsilon_0^{\text{eff}}(0)$ was tuned to resonance with $\varepsilon_1^{\text{eff}}(\pi/d)$ and coherent oscillations between both states, attributed to scattering, were observed after the forcing was switched on suddenly. In the Chicago experiments, tuning $\epsilon_1 - \hbar\omega < 0$ a hybridized band with two inequivalent minima $k_x = \pm q$ was created. Similar like in the case of the kinetically frustrated triangular lattice, repulsive interactions favor Bose condensation in one of the two minima, but not in both. Like in a ferromagnet, the experimentalists observed the formation

of spatial domains with $+q$ or $-q$ correlations (Parker *et al.*, 2013). The domain size was controlled by how fast the driving was switched on, with large domains obtained for slow ramps. In a subsequent experiment Bragg spectroscopy was used to measure the dispersion relation of the elementary Bogoliubov excitations of the system condensed into one of the minima (Ha *et al.*, 2015). It is phonon-like near the condensate momentum and can feature a local minimum at the second minimum of the effective dispersion relation of the non-interacting gas (see also Struck *et al.*, 2013). This structure reminds of a roton minimum resulting from long-ranged interactions.

The Harvard experiment (Bakr *et al.*, 2011) was performed in a rather deep lattice, where interactions are strong and band coupling can be understood on the level of a single site. By employing a modulation of the lattice depth in one direction, the lowest-band Wannier orbital was coupled to states of the same parity in this direction. The resonance frequency for coupling to the second excited state ($\alpha = 2$) was found to depend crucially on the on-site occupation of both states as a consequence of strong orbital-dependent interactions. This allows to engineer number-selective adiabatic passages, where a single particle is transferred to the excited band. In particular, by slowly ramping down the driving frequency, a sequence of such processes subsequently transfers all, but a single particle to the excited band, irrespective of the initial occupation. In this way an algorithmic cooling procedure was implemented: A state with an arbitrary number of atoms ≥ 1 in the lowest Wannier orbital on every site is eventually transformed into a state with one atom in the lowest Wannier orbital per site. Entropy has been transferred to an excited band, from where it can be removed by selectively taking away the excited atoms.

H. Floquet topological insulators

All the experiments discussed here so far, rely on high-frequency forcing, where $\hbar\omega$ is large compared to the tunneling matrix elements. This is different for a class of recent proposals for the Floquet engineering of lattice systems with topologically non-trivial band structures (Cayssol *et al.*, 2013; Kitagawa *et al.*, 2010; Lindner *et al.*, 2012; Oka and Aoki, 2009). These schemes, known as *Floquet topological insulators*, rely on driving frequencies that are only moderately larger than the tunneling matrix elements. The prototype of a Floquet topological insulator was originally proposed for graphene irradiated with circularly polarized light (Oka and Aoki, 2009). It is based on the observation that a hexagonal tight-binding lattice subjected to a circular force (48) possesses an effective band structure with a gap separating two bands with opposite Chern numbers ± 1 . Recently, this Floquet topological band structure has been realized and probed in two different experimental platforms. In a first exper-

iment with photons in a hexagonal array of optical wave guides, the chiral transport of localized particles at the boundary of the system was observed *in situ* (Rechtsman *et al.*, 2013). This is a signature of the chiral edge states related to Chern bands via the bulk-boundary correspondence (Hasan and Kane, 2010; Qi and Zhang, 2011). The second experiment was conducted by Jotzu *et al.*, 2014 in Esslinger's group in Zurich with ultracold fermionic atoms in a shaken hexagonal-like brick-wall lattice (Jotzu *et al.*, 2014). Here a finite Hall conductivity of the bulk system was measured.

A hexagonal lattice with isotropic nearest-neighbor tunneling [Fig. 5(b), solid lines] subjected to circular forcing (48) is described by the Hamiltonian (30) with time-dependent Peierls phases $\theta_{\ell'\ell}(t) = K \sin(\omega t - \varphi_{\ell'\ell})$. Here $K = Fd$ and the driving phase $\varphi_{\ell'\ell}$ is directly determined by the spatial direction of tunneling. In the high-frequency limit $\hbar\omega \gg J$, $\hat{H}'(t)$ can be approximated by its time average giving rise to effective tunneling matrix elements (23) between nearest neighbors. However, if the frequency is lowered, also the second-order term $\hat{H}_F^{(2)}$ in the high-frequency expansion (15) becomes relevant. Its contribution to the effective Hamiltonian \hat{H}_F results from processes where a particle tunnels twice during one driving period. Using Eq. (16) with $\hat{H}_m = -\sum_{\langle\ell'\ell\rangle} J\mathcal{J}_m(K/\hbar\omega)\hat{a}_{\ell'}^\dagger\hat{a}_\ell$, in second order one finds the kinetics to be described by the approximate effective Hamiltonian (Kitagawa *et al.*, 2011)

$$\begin{aligned} \hat{H}_F &\approx \hat{H}_F^{(1)} + \hat{H}_F^{(2)} \\ &= -J_{\text{eff}}^{(1)} \sum_{\langle\ell'\ell\rangle} \hat{a}_{\ell'}^\dagger\hat{a}_\ell - J_{\text{eff}}^{(2)} \sum_{\langle\langle\ell'\ell\rangle\rangle} e^{-i\sigma_{\ell'\ell}\theta} \hat{a}_{\ell'}^\dagger\hat{a}_\ell. \end{aligned} \quad (66)$$

Here $J_{\text{eff}}^{(1)} = J\mathcal{J}_0(K/\hbar\omega)$, $J_{\text{eff}}^{(2)} \simeq \sqrt{3}[J\mathcal{J}_1(K/\hbar\omega)]^2/\hbar\omega$ (neglecting terms with $m \geq 2$), $\theta = \pi/2$ and next-nearest-neighbor pairs $\langle\langle\ell'\ell\rangle\rangle$ with $\sigma_{\ell'\ell} = 1$ (-1) for tunneling in anticlockwise (clockwise) direction around a hexagonal plaquette.¹⁰ This model is the paradigmatic Haldane model, the prototype of a topological Chern insulator (Haldane, 1988). For finite next-nearest neighbor tunneling matrix elements the band structure acquires a gap separating two bands of opposite Chern number ± 1 . By introducing an energy difference Δ_{AB} between both sublattices *A* and *B* [Fig. 5(b)], the Chern numbers vanish when at $|\Delta_{AB}| = \Delta_{AB}^{(c)}$ the band gap closes. $|\Delta_{AB}^{(c)}|$

is maximum, $\approx 2.6|J_{\text{eff}}^{(2)}|$, for $\theta = \pm\pi/2$ and vanishes for $\theta = 0, \pi$.

In the Zurich experiment a distorted optical hexagonal lattice (a brick-wall lattice) with a tunable off-set Δ_{AB} is filled with spin-polarized (i.e. non-interacting) fermions (Jotzu *et al.*, 2014). An elliptical force $\mathbf{F}(t) = F[\cos(\omega t)\mathbf{e}_x + \cos(\omega t - \varphi)\mathbf{e}_y]$ is applied via lattice shaking. The system is described by an anisotropic effective model, whose phase diagram resembles that of the Haldane model with φ playing a role similar to θ . This phase diagram is mapped out by measuring the Hall response of the system.

I. Floquet engineering of interactions

In most of the experiments described above, periodic forcing was employed to effectively modify the single-particle Hamiltonian of the system, describing tunneling between neighboring lattice sites or the coupling between different Bloch bands. In contrast, the on-site interactions among the particles were not altered significantly by the driving. Exceptions are given by the experiments of Greiner's group discussed above. Here interactions were strong enough to shift the resonance condition for “photon”-assisted processes, tunneling (Chen *et al.*, 2011; Ma *et al.*, 2011) or band coupling (Bakr *et al.*, 2011), so that they became occupation-number selective. In this way tunneling or band coupling are not described by single-particle terms in the effective Hamiltonian anymore, which are quadratic in the annihilation and creation operators, and must be viewed as a form of interactions.

It is an interesting prospect to combine such a technique with driving schemes for the creation of artificial gauge fields as we discussed them in Sec. III.F (Bermudez and Porras, 2015; Cardarelli *et al.*, 2016; Sträter *et al.*, 2016). For that purpose one has to consider a lattice system, where the strong energy off-sets that have to be overcome by resonant “photon”-assisted tunneling are determined not only by static external potentials, but also by the strong interactions among the particles. Choosing the resonance condition $U = \nu\hbar\omega + \delta U$, with $|\delta U| \ll \hbar\omega$ between the Hubbard parameter for on-site interactions and the driving frequency, tunneling from site ℓ to site ℓ' corresponds to a potential energy change of an integer number $\nu_{\ell'\ell}$ of quanta $\hbar\omega$. Considering, e.g., spinless bosons, from Eq. (21) one obtains $\nu_{\ell'\ell} = \nu'_\ell - \nu_\ell + \nu[n_{\ell'} - (\nu_\ell - 1)]$, with site occupations n_ℓ and $n_{\ell'}$ before the tunneling event. For $\hbar\omega \gg J$, tunneling is suppressed for $\nu_{\ell'\ell} \neq 0$, unless it is reestablished via “photon”-assisted tunneling, giving rise to number-dependent effective tunneling parameters $J_{\ell'\ell}^{\text{eff}}(n_{\ell'}, n_\ell)$. The system is then described by an approximate effective Hamiltonian that, in rotating wave

¹⁰ Within the second-order Floquet-Magnus expansion of the Floquet Hamiltonian (18) the amplitude of the next-nearest-neighbor tunneling matrix elements depends on the direction of tunneling, so that the single-particle band-structure breaks the discrete rotational symmetry of the hexagonal lattice. This is an artifact of the approximation related to the fact that the driving phase in *x* and *y* direction differs by $\pi/2$ for circular forcing (Eckardt and Anisimovas, 2015). It illustrates the discussion following Eq. (19).

approximation, takes the form

$$\hat{H}_{\text{eff}} = - \sum_{\langle \ell' \ell \rangle} \hat{a}_{\ell'}^\dagger \hat{a}_\ell J_{\ell' \ell}^{\text{eff}}(\hat{n}_{\ell'}, \hat{n}_\ell) + \frac{U_{\text{eff}}}{2} \sum_{\ell} \hat{n}_\ell(\hat{n}_\ell - 1). \quad (67)$$

The effective Hubbard parameter is given by the non-resonant part of the interactions, $U_{\text{eff}} = \delta U = U - \nu \hbar \omega$, which is not integrated out when transforming to the rotating frame and whose magnitude and sign can be controlled by the driving frequency (this is true also for fermionic systems).

Bermudez and Porras, 2015, proposed such schemes, where the “photon”-assisted tunneling is induced by a moving-secondary-lattice as described in Sec. III.F.1. They lead to effective tunneling matrix elements described by Eq. (57), with $\nu_{\ell' \ell}$ replaced by an operator involving the occupation numbers of the particles. In this way they show, among others, how to engineer models where the magnetic field felt by one atomic species depends dynamically on the state of another species. Moreover, Sträter *et al.*, 2016 describe how to realize the physics of one-dimensional lattice anyons by inducing photon-assisted tunneling via asymmetric lattice shaking (see Sec. III.F.2). They use a mapping of the anyons to bosons with number-dependent tunneling parameters $J_{\ell+1, \ell} = |J|e^{i\theta\hat{n}_{\ell+1}}$ and $J_{\ell-1, \ell} = |J|e^{-i\theta\hat{n}_\ell}$, which had been exploited already in a previous proposal based on Raman-assisted tunneling (Keilmann *et al.*, 2010). Finally, Cardarelli *et al.*, 2016, propose a scheme based on the fact that “photon”-assisted tunneling induced by a sinusoidal modulation of the tunneling matrix element (as they can be induced by a modulation of the lattice depth) gives rise to single-“photon” transitions only. This can be seen from that fact that Eq. (47) describes non-zero effective tunneling matrix elements for $|\nu| \leq 1$ only. Thus, superimposing sinusoidal modulations at different frequencies, one can individually address tunneling processes corresponding to different number-dependent energy off-sets, with the amplitude and the phase of the effective tunneling matrix elements directly corresponding to the amplitude and the phase of the modulation.

An alternative approach for achieving number-dependent tunneling matrix elements consists in a modulation of the interaction strength (Gong *et al.*, 2009), as it can be achieved in a system of ultracold atoms by employing a magnetic Feshbach resonance, giving rise to a time-dependent Hubbard parameter $U(t) = U_0 + U_{\text{dr}}(t)$ with $U_{\text{dr}}(t + T) = U_{\text{dr}}(t)$ and $\int_0^T dt U_{\text{dr}}(t) = 0$. In this way the energy of multiply occupied lattice sites is modulated in time, so that for spinless bosons tunneling from ℓ to ℓ' is connected to an energy change of $U(t)[n_{\ell'} - (n_{\ell} - 1)]$. Thus, for $U_0 \ll J$ and sinusoidal forcing $U_{\text{dr}}(t) = U_1 \cos(\omega t)$, the effective tunneling matrix elements $J_{\ell' \ell}^{\text{eff}}(n_{\ell'}, n_{\ell})$ are given by Eq. (23) with K replaced by $K_{\ell' \ell} = U_1[n_{\ell'} - (n_{\ell} - 1)]$. Signatures of this effect, which was first described theoretically by Gong

et al., 2009, have recently been observed experimentally in Nägerl’s group (Meinert *et al.*, 2016) by measuring the number of multiply occupied sites after a quench. It is moreover, proposed to use this principle to engineer exotic many-body states of matter (Greschner *et al.*, 2014; Liberto *et al.*, 2014; Rapp *et al.*, 2012).

Another driving-induced modification of the interactions is described by higher-order corrections of the effective Hamiltonian in high-frequency approximation (16). If the Hubbard interactions are time-independent, so that they contribute to the Fourier component \hat{H}_0 of the Hamiltonian only, the leading correction involving the interactions appears in the third-order term $\hat{H}_F^{(3)}$.¹¹ It reads (Eckardt and Anisimovas, 2015)

$$\hat{H}_F^{(\text{int}, 3)} = \sum_{m \neq 0} \frac{[\hat{H}_{-m}, [\hat{H}_{\text{int}}, \hat{H}_m]]}{2(m\hbar\omega)^2}, \quad (68)$$

where \hat{H}_m denote the Fourier components of the single-particle Hamiltonian, so that $\hat{H}_F^{(\text{int}, 3)} \propto UJ^2/(\hbar\omega)^2$. When $U \gg J$, this term can matter in Floquet topological systems (Sec. III.H), where the frequency is moderately large only, such that effective next-nearest-neighbor tunneling matrix elements $J_{\text{eff}}^{(2)} \propto J^2/(\hbar\omega)$ [Eq. 66] play a crucial role. For the model of Sec. III.H, the \hat{H}_m are specified above Eq. (66). The effect of $\hat{H}_F^{(\text{int}, 3)}$ is to “smear-out” the interactions. It creates effective nearest-neighbor interactions $\frac{V_{\text{eff}}}{2} \sum_{\langle \ell' \ell \rangle} \hat{n}_{\ell'} \hat{n}_\ell$ (at the cost of lowering the on-site interactions to $U - zV_{\text{eff}}/2$ with coordination number z) and also gives rise to density-assisted and two-particle tunneling (Eckardt and Anisimovas, 2015). Numerical studies based on the exact diagonalization (Anisimovas *et al.*, 2015; Račiūnas *et al.*, 2016) suggest that this smearing out tends to have a negative impact on the possible stabilization of fractional-Chern- insulator states in Floquet topological band structures recently proposed by Grushin *et al.*, 2014.

IV. THE FLOQUET PICTURE

So far, we have argued that a simple high-frequency approximation provides a suitable description of a variety of recent experiments, where ultracold atoms in optical lattices were controlled by means of periodic driving. In this section we will discuss the limitations of this approximation and effects beyond it. This requires a treatment in terms of the extended Floquet Hilbert space.

¹¹ Within the Floquet-Magnus expansion of the Floquet Hamiltonian (18) an interaction correction $\propto JU/(\hbar\omega)$ appears already in the second-order term (Bukov *et al.*, 2015a; Verdeny *et al.*, 2013) [$\hat{H}_{t_0}^{F(2)}$ in Eq. (19) contains \hat{H}_{int} through \hat{H}_0]. However, this correction results from the expansion of the unitary micro-motion operator and thus does not alter the spectrum on the order of $JU/(\hbar\omega)$ (see discussion below Eq. (19)).

A. Extended Floquet Hilbert space

By plugging the Floquet state given by Eq. (14) into the Schrödinger equation (3), one obtains $[\hat{H}(t) - i\hbar d_t]|u_{nm}(t)\rangle = \varepsilon_{nm}|u_{nm}(t)\rangle$. As was pointed out by Sambe, 1973, this equation can be interpreted as the eigenvalue problem of the hermitian *quasienergy operator*

$$\hat{Q}(t) = \hat{H}(t) - i\hbar d_t, \quad (69)$$

acting in an extended Hilbert space $\mathcal{F} = \mathcal{H} \otimes \mathcal{T}$. This Floquet space is the product space of the physical state space \mathcal{H} and the space of time-periodic functions (with period T) \mathcal{T} . In \mathcal{F} the scalar product combines the scalar product of \mathcal{H} with time averaging and reads

$$\langle\langle u|v\rangle\rangle = \frac{1}{T} \int_0^T dt \langle u(t)|v(t)\rangle. \quad (70)$$

We will use a double ket $|u\rangle\rangle$ for elements of \mathcal{F} ; the corresponding state at time t in \mathcal{H} is denoted $|u(t)\rangle$. Vice versa, a state $|v(t)\rangle = |v(t+T)\rangle$, including its full periodic time dependence, is written as $|v\rangle\rangle$ when considered as element of \mathcal{F} . Likewise, an operator acting in \mathcal{F} will be indicated by an overbar to distinguish it from operators acting in \mathcal{H} , which are marked by a caret. For example, \bar{Q} denotes the quasienergy operator. Its eigenvalue problem is now written like

$$\bar{Q}|u_{nm}\rangle\rangle = \varepsilon_{nm}|u_{nm}\rangle\rangle. \quad (71)$$

In Floquet space $|u_{nm}\rangle\rangle$ and $|u_{nm'}\rangle\rangle$, defined by Eq. (13), constitute independent orthogonal solutions if $m' \neq m$, so that the quasienergy spectrum is periodic with period $\hbar\omega$. Despite this redundancy, working in \mathcal{F} has the advantage that one can use both methods and intuition developed for autonomous systems.

From a complete basis of orthogonal states $|\alpha\rangle$ of \mathcal{H} , we can construct a complete basis of orthogonal states $|\alpha m\rangle\rangle$ of \mathcal{F} , given by $|\alpha m(t)\rangle\rangle = |\alpha\rangle e^{im\omega t}$ with integer m . In terms of these basis states the quasienergy operator possesses matrix elements

$$\langle\langle \alpha' m' | \bar{Q} | \alpha m \rangle\rangle = \langle \alpha' | \hat{H}_{m'-m} | \alpha \rangle + \delta_{m'm} \delta_{\alpha'\alpha} m \hbar \omega. \quad (72)$$

The matrix possesses a transparent block structure with respect to m . The diagonal blocks are determined by the time-averaged Hamiltonian \hat{H}_0 and shifted with respect to each other by integer multiples of $\hbar\omega$ in quasienergy. This structure resembles that of a quantum system coupled to a photon-like mode in the classical limit of large photon numbers. In this picture m plays the role of a relative photon number. The quasienergy eigenvalue problem (71) is, thus, closely related to the dressed-atom picture (Cohen-Tannoudji *et al.*, 1998) for a quantum system driven by coherent radiation (Eckardt and Holthaus, 2008b). Therefore, m is often called the “photon” number and the matrix elements of \hat{H}_m are said to describe

m -“photon” processes. A unitary operator \bar{U}_F that block diagonalizes \bar{Q} with respect to the “photon” index m in \mathcal{F} corresponds directly to a time-periodic unitary micromotion operator $\hat{U}_F(t)$ in \mathcal{H} , as it appears in Eqs. (4) and (5). It produces diagonal blocks given by the effective Hamiltonian (4),

$$\langle\langle \alpha' m' | \bar{U}_F^\dagger \bar{Q} \bar{U}_F | \alpha m \rangle\rangle = \delta_{m'm} \left(\langle \alpha' | \hat{H}_F | \alpha \rangle + \delta_{\alpha'\alpha} m \hbar \omega \right). \quad (73)$$

B. High-frequency approximation

If $\hbar\omega$ is large compared both to the spectral width \hat{H}_0 and the matrix elements of the $\hat{H}_{m \neq 0}$, states of different subspaces m are energetically well separated and coupled only weakly to each other. It is, therefore, a reasonable approximation to neglect the off-diagonal blocks of the quasienergy operator (72) and to approximate the effective Hamiltonian \hat{H}_F by the time-averaged Hamiltonian \hat{H}_0 . Corrections, resulting from the perturbative admixture of states with $m' \neq m$ to those of the subspace m , can be obtained systematically by means of degenerate perturbation theory. The high-frequency expansion (15) is equivalent to such a perturbative approach, where the “photonic” part $\delta_{\alpha'\alpha} \delta_{m'm} m \hbar \omega$ of the matrix (72) constitutes the unperturbed problem and the Hamiltonian (its Fourier components \hat{H}_m) the perturbation (Eckardt and Anisimovas, 2015).

The perturbative approach underlying the high-frequency expansion (15) can be expected to converge only as long as the quasienergy levels originating from different unperturbed subspaces m remain energetically well separated. This rough statement is similar to the rigorous convergence criterion for the Floquet-Magnus expansion given by Casas *et al.*, 2000 (see discussion at the end of section II). In a large system of many particles reasonable driving frequencies $\hbar\omega$ will always be smaller than the spectral width of the full time-averaged Hamiltonian \hat{H}_0 , so that the high-frequency expansion cannot be expected to converge (unless the state space of the system is effectively divided into small subspaces due to symmetry or localization). Nevertheless, even in this case the high-frequency approximation (34) can still provide a suitable description of a driven many-body system on a finite time scale, provided $\hbar\omega$ is large compared to typical intensive energy scales, such as the tunneling parameter J or the Hubbard interaction U for a driven Hubbard model (Eckardt *et al.*, 2005). This statement is not surprising given the fact that in the previous section III we were able to explain a variety of experimental observations in terms of the high-frequency approximation. On longer times, deviations from the high-frequency approximation will, however, eventually make themselves felt as heating.

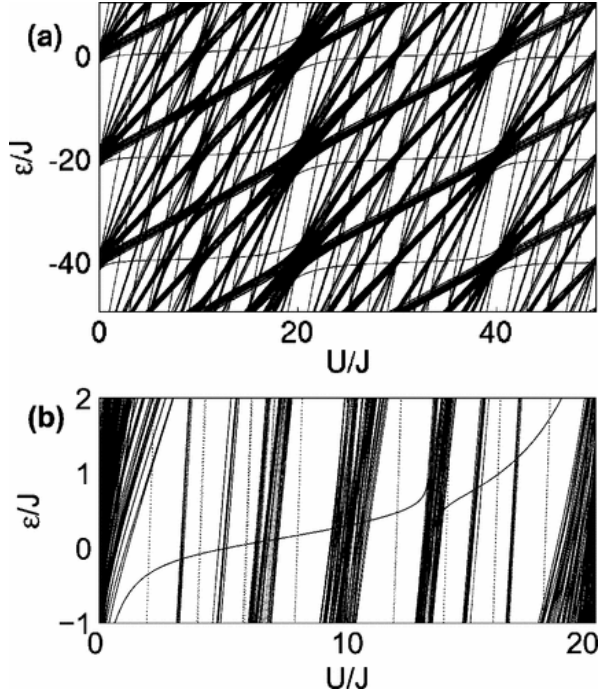


FIG. 6 Quasienergy spectrum of small Bose Hubbard chain (five particles on five sites), subjected to a sinusoidal force of frequency $\hbar\omega/J = 20$ and amplitude $K/\hbar\omega = 2$. (b) Zoom into (a). (taken from Eckardt and Holthaus, 2008a)

C. Heating and long-time limit

In order to illustrate the break-down of the high-frequency approximation, let us discuss a specific example (Eckardt and Holthaus, 2008a). Fig. 6 shows the exact quasienergy spectrum of a small Bose-Hubbard chain subjected to a sinusoidal force of frequency $\hbar\omega/J = 20$, plotted versus the interaction strength U/J . For $U/J \gg 1$, the spectrum of \hat{H}_0 consists of bands whose energies increase linearly with U . These bands lie above the horizontal ground-state level, corresponding to a Mott-insulator-like state with one particle localized at every lattice site. They contain states characterized by delocalized particle-hole excitations. The spectrum of \hat{H}_0 can clearly be identified in Fig. 6, as well as copies of it, shifted by $-\hbar\omega$, $-2\hbar\omega$, \dots . When states belonging to different copies (“photon” numbers m) become degenerate, this leads to the formation of avoided level crossings, the size of which reflects the coupling strength. Near $U = \hbar\omega = 20J$ and $U = 2\hbar\omega = 40J$, the ground state participates in a large avoided-crossing-like feature (involving many bands), associated with the resonant creation of a particle-hole pair of energy U . The size of this feature is determined by the coupling matrix element J associated with the creation of a particle-hole pair. For $U < \hbar\omega$, a smaller avoided crossing is visible in subfigure (b) near $U = 2\hbar\omega/3 \approx 13J$. It can be attributed to the creation of two coupled particle-hole excitations

of energy $3U$ in a two-“photon” process. The size of the avoided crossing, which reflects the coupling matrix element, is of the order of $\sim J^2/(\hbar\omega)$. Whereas the numerator of this factor results from the fact that two tunneling processes are required to create a two particle-hole pairs, the denominator indicates that the transition occurs via intermediate states (having a single-particle-hole pair) that are separated by a large energy $\sim \hbar\omega$ (Eckardt and Anisimovas, 2015). For even smaller values of U , the $m = 0$ ground state will cross even higher lying bands of the $m < 0$ copies, which contain states with three and more particle-hole excitations. The corresponding coupling matrix elements are $\sim J^{j+1}/(\hbar\omega)^j$ with $j \geq 2$ and the resulting avoided crossings are hardly visible in Fig. 6. Generally, the larger $\hbar\omega$ compared to both U and J , the more complex are the collective excitations at energies $\hbar\omega$ and the smaller are the respective coupling matrix elements.

The formation of an avoided crossing, where the Floquet states of different subspaces m and m' hybridize, cannot be captured by a perturbation theory describing the system in terms of eigenstates labeled by the quantum number m . Their presence indicates that the high-frequency expansion (15), which can be obtained from such a perturbative approach (Eckardt and Anisimovas, 2015), does not converge. However, we have seen that when both J and U are sufficiently small with respect to $\hbar\omega$, the coupling between degenerate states originating from different subspaces m will be very small. Therefore, deviations from the high-frequency approximation will make themselves felt on a large time scale t_h only. These deviations can be viewed as heating. In the driven Bose-Hubbard model with strong interactions $U \gg J$ discussed in the previous paragraph they correspond to the creation of particle-hole excitations (Eckardt and Anisimovas, 2015; Eckardt and Holthaus, 2008a), for weakly interacting systems they correspond to energy-nonconserving two-particle scattering (Bilitewski and Cooper, 2015a,b; Choudhury and Mueller, 2014, 2015; Genske and Rosch, 2015). For a numerical study of such heating see Poletti and Kollath, 2011.

As long as the duration of an experiment is short compared to the heating time t_h , it can be described by the high-frequency approximation (15). For lattice systems with a bound local state space, *e.g.* fermionic Hubbard or spin models, it was shown very recently that t_h increases exponentially with the driving frequency (Abanin *et al.*, 2015c; Kuwahara *et al.*, 2016; Mori *et al.*, 2016) and that the Floquet-Magnus expansion (18) provides at least an asymptotic expansion for the Floquet Hamiltonian with an optimal order μ_{cut} of truncation (Kuwahara *et al.*, 2016).

The spectrum shown in Fig. 6 has been obtained for a small system of five particles on five lattice sites only. Approaching the thermodynamic limit, where the system size and the particle number are taken to infinity at

fixed density, the bands of the spectrum \hat{H}_0 will approach a continuum and new bands will be created at high energies. The quasienergy spectrum of the system, hosting an exponentially large number of quasienergy levels in each Brillouin zone (interval of width $\hbar\omega$), will approach a highly structured continuum. In this limit, the full effective Hamiltonian will be a very complex object, whose eigenstates, the Floquet modes, are superpositions of states having very different energies. This scenario explains, why a description in terms of the simple expressions provided by the high-frequency approximation (15) is a suitable approach for Floquet engineering, despite the fact that such a description is valid for times $t \ll t_h$ only.

The existence of a heating time t_h implies that, when a periodically driven system is subjected to a quench, *i.e.* a sudden change of a parameter like the driving amplitude, the subsequent relaxation dynamics can consist of two stages. After the quench, the system can first relax on a time scale t_r to an equilibrium-like state with respect to the effective Hamiltonian in high-frequency approximation (15), before the intrinsic heating due to the periodic forcing sets in on the time scale t_h . Obviously this scenario requires $t_r \ll t_h$. Such a behavior, which has first been discussed already by Maricq, 1982 can be interpreted as a form of *prethermalization*. It is investigated theoretically in several recent papers (Abanin *et al.*, 2015a,b,c; Bukov *et al.*, 2015b; Canovi *et al.*, 2016; Kuwahara *et al.*, 2016; Mori *et al.*, 2016).

Another intriguing question concerns the relaxation of periodically driven quantum systems on time scales much longer than the heating time. From Eq. (9) we can infer that for a pure state $|\psi(t)\rangle$ the time evolution of the expectation value $O(t) = \langle \psi(t) | \hat{O} | \psi(t) \rangle$ of an observable \hat{O} can be written like

$$O(t) = \sum_{n',n} c_{n'}^* c_n e^{\frac{i}{\hbar}(\varepsilon_{n'} - \varepsilon_n)t} \langle u_{n'}(t) | \hat{O} | u_n(t) \rangle. \quad (74)$$

Russomanno *et al.*, 2012, have argued that a relaxation to a steady state will correspond to the dephasing of the off-diagonal terms with $n' \neq n$, so that asymptotically in the long-time limit, after a relaxation has occurred, the expectation values are described by

$$O(t) \simeq \sum_n |c_n|^2 \langle u_n(t) | \hat{O} | u_n(t) \rangle, \quad (75)$$

corresponding to the diagonal ensemble (Dziarmaga, 2010; Polkovnikov *et al.*, 2011) with respect to the Floquet states. This implies that $O(t)$ becomes time-periodic, $O(t+T) = O(t)$; the system synchronizes with the driving. Moreover, Lazarides *et al.*, 2014b have shown that for non-interacting (integrable) systems the asymptotic expectation values can be obtained using the principle of entropy maximization, under the constraint that the mean occupations $\langle \hat{n}_i \rangle$ of the single-particle Floquet states i retain their initial values. The

asymptotic state is, thus, captured by a periodic generalized Gibbs ensemble, so that for typical observables $O(t) \simeq \text{tr}\{\rho(t)\hat{O}\}$ with time-periodic density matrix $\hat{\rho}(t) \propto \hat{U}_F(t) \exp(-\sum_i \lambda_i \hat{n}_i) \hat{U}_F^\dagger(t)$. The number of parameters λ_i required to control the integrals of motion $\langle \hat{n}_i \rangle$ grows only linearly with the system size. It is much lower than the number of coefficients c_n appearing in Eq. (75), which grows exponentially with the system size (since n labels the many-body Floquet states, in this case Fock states of the single-particle Floquet states, $n = \{n_i\}$). The arguments sketched here in the context of Floquet systems are very similar to those employed for the relaxation of isolated autonomous systems (Dziarmaga, 2010; Polkovnikov *et al.*, 2011). An interesting exception of the behavior described above has recently been discussed by Else *et al.*, 2016, who constructed a periodically driven model system that in the thermodynamic limit relaxes to an asymptotic state, dubbed *Floquet time crystal*, with $O(t) \neq O(t+T)$, but $O(t) = O(t+kT)$ with integer k . This behavior is associated with a spontaneous breaking of the discrete time translational symmetry, since the time required to reach a periodic state with $O(t) = O(t+T)$ grows exponentially with the system size.

For non-integrable Floquet systems, it is believed that the system approaches a state described by an infinite-temperature ensemble (D'Alessio and Rigol, 2014; Lazarides *et al.*, 2014a). In the sense of eigenstate thermalization, for typical observables almost all many-body Floquet modes $|u_n(t)\rangle$ appearing in Eq. (75) are conjectured to give rise to the same infinite-temperature expectation values for typical observables, $\langle u_n(t) | \hat{O} | u_n(t) \rangle \simeq O$ independent of n . Roughly speaking, due to the lack of energy conservation, the many-body Floquet states are formed by the hybridization of many eigenstates of \hat{H}_0 at all available energy scales so that their properties can be computed statistically. However, also possible exceptions to this behavior have been discussed (Abanin *et al.*, 2014; Lazarides *et al.*, 2015; Ponte *et al.*, 2015), including systems featuring many-body localization (for which the size of the state space is effectively reduced via the segmentation into local subspaces). The work on the relaxation of isolated Floquet systems sketched in the last three paragraphs is very recent and it will be interesting to follow further developments and possible experimental studies.

Above, we have mentioned that the heating time t_h is expected to increase exponentially with the driving frequency for systems with a bound local state space. In experiments with ultracold atoms in driven optical lattices, this condition is never fulfilled due to the presence of excited orbital states spanning higher-lying Bloch bands (which are not included in the low-energy tight-binding description in terms of a Hubbard model). While an effective description in terms of low-energy degrees of freedom is very natural in non-driven systems, the trunca-

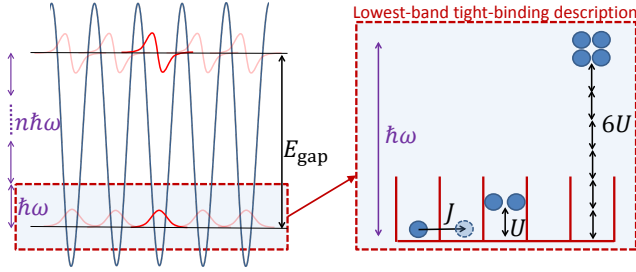


FIG. 7 In periodically driven optical lattices, heating occurs due to the resonant creation of high-energy excitations, either interband excitations (left) or collective intraband-excitations (right, illustrated using the example of a large bosonic site occupation). The time scales for these processes should be large compared to the duration of the experiment.

tion of high-energy states is a delicate issue in periodically driven systems already on the single-particle level (Hone *et al.*, 1997). In a periodically driven optical lattice the driving frequency is typically chosen such that $\hbar\omega$ lies well below the band gap E_{gap} that separates excited orbital states from the tight-binding state space spanned by one low-energy Wannier state in each lattice minimum. However, interband excitations can still occur via n -“photon” processes (Fig. 7, left). The smaller n , the larger will be the coupling matrix element for such interband-heating processes. Thus, by increasing the driving frequency, the heating rate associated with the resonant creation of collective intraband excitations (7, right), as we discussed them above using the example presented in Fig. 6, might decrease. However, at the same time the heating rate due to interband excitations tends to increase with the driving frequency. Floquet engineering with ultracold atomic quantum gases in optical lattice, therefore, requires that there is a window of intermediate frequencies for which neither intraband nor interband heating is relevant on the time scale of the experiment. Interband transitions can occur both as a consequence of single-particle processes (Drese and Holthaus, 1997b; Holthaus, 2015) or two-particle scattering (Choudhury and Mueller, 2014, 2015). For strong driving, multi-“photon” interband excitations with n as large as nine have recently been observed experimentally and explained in terms of single-particle transitions (Weinberg *et al.*, 2015). Arguments based on perturbation theory suggest that the rate for such heating processes is suppressed exponentially with $n \approx E_{\text{gap}}/(\hbar\omega)$, provided the driving amplitude remains below a threshold value (Sträter and Eckardt, 2016).

D. Anomalous topological edge states

The $\hbar\omega$ -periodic structure of the quasienergy spectrum of periodically driven quantum systems reflects the in-

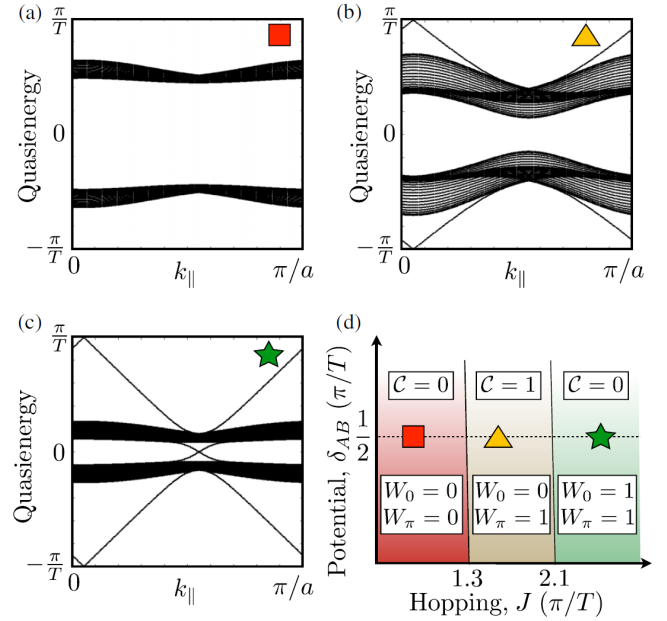


FIG. 8 (a-c) Floquet spectra of periodically driven square lattice defined in Fig. 9(a) for the parameters specified in (d). (d) Phase diagram versus tunneling parameter J and sublattice off-set δ_{AB} (in units of $\hbar\omega/2$). Phases are characterized by the winding numbers W_ε for the bulk gaps at quasienergy ε ; the Chern number of the upper (lower) band is given by C ($-C$). (taken from Rudner *et al.*, 2013)

terplay between the dynamics occurring within a driving period (associated with energy scales larger than $\hbar\omega$) with that happening on longer time scales (associated with energy scales smaller than $\hbar\omega$). The possibility that heating occurs on a long time scale due to the resonant coupling of energetically far distant states, discussed in the previous section, is one example of such an interplay. Another, more subtle effect related to this interplay is the existence of anomalous topological edge states in periodically driven systems (Jiang *et al.*, 2011; Kitagawa *et al.*, 2010, 2012; Rudner *et al.*, 2013). Without making an attempt to give a complete overview of the numerous recent works on this subject, we will briefly sketch the phenomenon in the context of non-interacting spinless particles in a two-dimensional lattice, following Rudner *et al.*, 2013.

Consider a periodically driven two-dimensional tight-binding lattice with B sublattice states. For periodic boundary conditions the quasienergy spectrum will possess B Floquet-Bloch bands that shall be separated by gaps. When the translational symmetry is broken by open boundary conditions, the system can feature chiral edge states that reflect the topological nature of the bulk band structure. Spatially these states are localized at the boundary (in the direction perpendicular to it), but delocalized in the direction parallel to it. They transport particles in one direction along the boundary only (de-

finer by their chirality). Figs. 8(a-c) show quasienergy spectra for a driven two-dimensional lattice of finite extent with two sublattice states for different parameters. The spectra are plotted versus the quasimomentum k_{\parallel} parallel to two opposite edges (Rudner *et al.*, 2013). The bulk bands have a finite width according to their dispersion in the perpendicular direction. Sometimes neighboring bulk bands are connected by lines traversing a band. These lines form one-dimensional bands corresponding to chiral edge states. They come in pairs of opposite slope (indicating opposite velocity) corresponding to the two opposite edges.

Like in autonomous systems, the presence or absence of chiral edge states is connected to the topological properties of the bulk (bulk-boundary correspondence, see *e.g.* Hasan and Kane, 2010 and Qi and Zhang, 2011). The difference between the number of edge bands entering a bulk band b from below and that exiting it above is dictated by the Chern number C_b of that band [Eq. (60)], which is a bulk property. However, there is one important difference that distinguishes periodically driven from autonomous systems. As a consequence of the $\hbar\omega$ -periodic structure of the quasienergy spectrum, edge bands can exit the uppermost bulk band in the quasienergy interval $[-\hbar\omega/2, \hbar\omega/2]$ above and enter the lowermost bulk band from below [Figs. 8(b) and (c)] (Jiang *et al.*, 2011; Kitagawa *et al.*, 2010). This possibility implies that the system can feature chiral edge states even if all bulk bands have Chern number zero, like in Fig. 8(c). With that it also implies that the presence or absence of chiral edge states is not determined by the Chern numbers alone. This is illustrated by the fact that in both Figs. 8(a) and (c) the bands have identical Chern numbers, despite the respective absence and presence of edge modes. In contrast, in an autonomous systems the number of edge states in the gap above a certain bulk band b is given by $\sum_{\beta \leq b} C_{\beta}$, since no edge bands can enter the lowest band from below.

Rudner *et al.*, 2013, identify a winding number W_{ε} from the bulk properties of the system that determines the number of edge modes traversing the band gap containing the quasienergy ε , $n_{\text{edge}} = W_{\varepsilon}$. The difference $W_{\varepsilon'} - W_{\varepsilon}$ corresponds to the sum of the Chern numbers of the bands lying between the gaps at ε' and ε . The winding numbers associated with all bulk gaps give a complete topological description of a driven two-dimensional lattice. These topological invariants do not only depend on the time-evolution operator over one driving period, $\hat{U}(t_0+T, t_0)$ or $\hat{U}(T, 0)$ for definiteness. They also depend on the time-evolution *during* each period as it is captured by the function $\hat{U}(t) = \hat{U}(t, 0)$, that is they depend on the micromotion. The winding number is defined like

$$W_{\varepsilon} = \frac{1}{8\pi^2} \int dt dk_x dk_y \text{tr} \left(\hat{U}_{\varepsilon}^{\dagger} \partial_t \hat{U}_{\varepsilon} [\hat{U}_{\varepsilon}^{\dagger} \partial_{k_x} \hat{U}_{\varepsilon}, \hat{U}_{\varepsilon}^{\dagger} \partial_{k_y} \hat{U}_{\varepsilon}] \right), \quad (76)$$

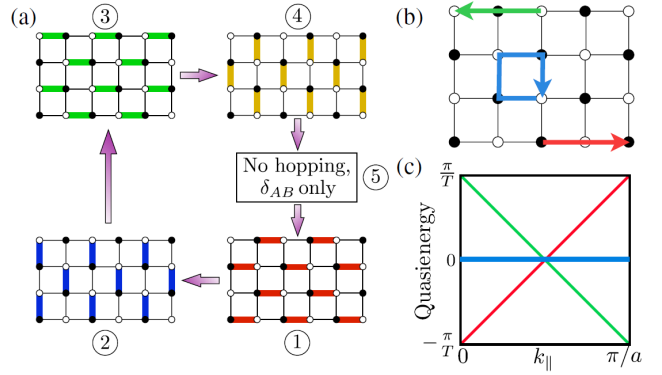


FIG. 9 (a) Simple model system on a square lattice with two sublattice states (open and filled circles). Each driving period is divided into five stages of duration $T/5$. During each stage either tunneling matrix elements J are present on the highlighted bonds or an energy offset δ_{AB} between both sublattices. (b) Dynamics of an initially site-localized particle during one driving cycle for fine-tuned parameters $J = (5/4)\hbar\omega$ and $\delta_{AB} = 0$ in the bulk (blue) and at the edges (green, red). (c) Quasienergy spectrum for parameters of (b). The bulk levels (blue) are dispersionless, whereas the levels for the chiral edge modes (red, green) wrap around the Brillouin zone with constant slope. (taken from Rudner *et al.*, 2013)

where $\hat{U}_{\varepsilon}(\mathbf{k}, t)$ is a unitary operator with $\hat{U}_{\varepsilon}(\mathbf{k}, T) = 1$. It has to be obtained by continuously deforming the single-particle time evolution operator $\hat{U}(t) = \hat{U}(\mathbf{k}, t)$ (in the sector with quasimomentum \mathbf{k}) in a way that the gap at ε is smoothly shifted to $\hbar\omega/2$ without being closed on the way. A concrete construction of a suitable operator $\hat{U}_{\varepsilon}(\mathbf{k}, t)$ for general $\hat{U}(\mathbf{k}, t)$ is given by Rudner *et al.*, 2013.

The dependence of the winding number on the micromotion has an interesting consequence for the bulk-boundary correspondence in Floquet systems: The quasienergy spectrum and the Floquet states (including the edge states) can be obtained from the time-evolution operator over one driving cycle $\hat{U}(T)$ by using Eq. (8). However, the operator $\hat{U}(T)$ computed for a translational invariant system, which represents the bulk properties, does not completely determine the properties of the edge states appearing at the boundary of a finite system. The edge states depend also on the micromotion of the bulk inherent in the time-dependence of the evolution operator $\hat{U}(t)$.

Rudner *et al.*, 2013, illustrate this effect using the specific model shown in Fig. 9(a). For fine-tuned parameters the dynamics during each driving cycle is simply that depicted in Fig. 9(b): In the bulk, a site-local particle moves around a closed circle and returns to its initial state. So while the micromotion in the bulk is non-trivial, the Floquet Hamiltonian \hat{H}_0^F , which describes/generates the stroboscopic dynamics in steps of the driving period T , vanishes in the bulk. At the edge of the system, the motion around the closed loop is not possible so that a particle is transported counter clockwise along the boundary

during each driving period, corresponding to the formation of a band of chiral edge states. Clearly, this edge dynamics results from the interplay of the bulk micromotion with the boundary of the system. The quasienergy spectrum is plotted in Fig. 9(c); while the trivial bulk dynamics over one driving period is reflected in a flat bulk dispersion, chiral edge bands with constant slope (representing the velocity of two lattice constants per driving period) wrap around the Brillouin zone.

The model system of Fig. 9(a) (without driving stage 5, though) and the emergence of chiral edge states was investigated recently in experiments with photonic wave guides (Maczewesky *et al.*, 2016; Mukherjee *et al.*, 2016). An implementation of a similar model defined on a hexagonal lattice (Kitagawa *et al.*, 2011) with ultracold atoms and the observation of chiral edge states at interfaces between spatial domains with different topological properties has been proposed by (Reichl and Mueller, 2014). Anomalous chiral edge states have, moreover, been observed in photonic networks (Gao *et al.*, 2016; Hu *et al.*, 2015). In the circularly forced hexagonal lattice (Jotzu *et al.*, 2014; Kitagawa *et al.*, 2011; Oka and Aoki, 2009), which we discussed in Sec. III.H, anomalous edge states appear for driving frequencies that are low enough to resonantly couple the two low-energy Bloch bands described by the Hubbard model (Usaj *et al.*, 2014), *i.e.* when the high-frequency approximation (15) breaks down. This is not surprising, since the effective Hamiltonian obtained within the high-frequency approximation (15) cannot describe effects related to the $\hbar\omega$ -periodic structure of the quasienergy spectrum, such as the anomalous topological edge states discussed in this section.

E. Two-time formalism

The concept of Floquet theory can be extended to capture also situations where the Hamiltonian is not perfectly periodic in time, *e.g.* when a parameter like the driving strength is varied (Breuer and Holthaus, 1989b; Peskin and Moiseyev, 1993; Pfeifer and Levine, 1983). For an arbitrary time-dependent Hamiltonian $\hat{H}(t)$, one can always define a time-periodic Hamiltonian $\hat{H}_\tau(t) = \hat{H}_\tau(t + T)$, with parametric dependence on a second time τ such that $\hat{H}(t) = \hat{H}_\tau(t)$. For example, for $\hat{H}(t) = \hat{H}_0 + p(t) \cos(\omega t) \hat{V}$, with slowly varying amplitude $p(t)$, we can set $\hat{H}_\tau(t) = \hat{H}_0 + p(\tau) \cos(\omega t) \hat{V}$. This choice is not unique, but for a “natural” description of the problem, the dependence on τ should be weak, slow, or limited to a finite interval in time. The quasienergy operator related to $\hat{H}_\tau(t)$ is given by

$$\hat{Q}_\tau(t) = \hat{H}_\tau(t) - i\hbar d_t. \quad (77)$$

Now a Schrödinger-type equation of motion

$$i\hbar d_\tau |\Psi_\tau\rangle = \bar{Q}_\tau |\Psi_\tau\rangle \quad (78)$$

for states in the extended Floquet Hilbert space can be postulated, where \bar{Q}_τ generates the evolution with respect to the time τ . A straightforward calculation shows that

$$|\psi(t)\rangle = |\Psi_t(t)\rangle, \quad (79)$$

with $|\Psi_\tau(t)\rangle$ being the \mathcal{H} -space representation of $|\Psi_\tau\rangle$, is a solution of the (actual) Schrödinger equation (3) of the Hamiltonian $\hat{H}(t)$ (Breuer and Holthaus, 1989b). This means that one can integrate Eq. (78) in \mathcal{F} in order to compute the time evolution of the system as it is described by the time-dependent Schrödinger equation (3). The initial condition has to obey $|\Psi_{t_0}(t_0)\rangle = |\psi(t_0)\rangle$, as can be achieved, *e.g.*, by setting $|\psi_{t_0}\rangle = \sum_\alpha \langle\psi(t_0)|\alpha\rangle |\alpha 0\rangle$. The two-time formalism provides a Floquet-space description of the time evolution generated by arbitrary time-dependent Hamiltonians $\hat{H}(t)$. Therefore, it constitutes a *Floquet picture* (Breuer and Holthaus, 1989a). Working in the Floquet picture is useful when the Hamiltonian is approximately time periodic.¹²

F. Adiabatic state preparation

A direct consequence of the evolution equation (78) is that one can apply the adiabatic principle to Floquet states and their quasienergies (Breuer and Holthaus, 1989b). In particular the transition probabilities associated with parameter variations through isolated avoided crossings of two quasienergy levels are captured by Landau-Zener theory. While for a slow (rapid) parameter variation the crossing is passed adiabatically (diabatically), a superposition of both states is created for intermediate rates.

An important protocol of Floquet engineering is the preparation of the ground state of the approximate effective Hamiltonian to be realized by Floquet engineering via a smooth parameter variation starting from the ground state of the undriven system. On the level of a description in terms of the high-frequency approximation (15), say in leading order $\hat{H}_F \approx \hat{H}_0$, the ideal dynamics should be adiabatic. However, as was discussed in section IV.C using the example of Fig. 6, the ground state of \hat{H}_0 will undergo avoided level crossings with excited states of energy $m\hbar\omega$. In the high-frequency regime these avoided crossings are tiny. For the high-frequency approximation to be valid, they should be passed diabatically, reflecting once more that the high-frequency approximation is valid on finite times only. Thus, the ideal preparation

¹² A suitable description of problems where the driving frequency itself varies in time is obtained by a temporal scaling transformation (Drese and Holthaus, 1999).

should be based on an *effectively adiabatic* dynamics, defined as a mixture of adiabatic dynamics with respect to the high-frequency approximation and diabatic dynamics with respect to resonant coupling neglected in this approximation (Eckardt and Holthaus, 2008a).

V. CONCLUSION AND OUTLOOK

We have seen that periodic forcing can be powerful tool for the engineering many-body systems of ultra-cold atoms in optical lattices with tailor-made properties. While a basic description of such Floquet engineering can often be given in terms of simple (high-frequency single-band) approximations, the justification of these approximations is a more subtle issue. Future research will, therefore, not only be concerned with novel control schemes, but also with the stability of Floquet systems towards heating. Efficient strategies for suppressing heating will also be crucial for another ambitious goal, the preparation of strongly correlated topologically ordered states of matter, such as fractional Chern insulators.

An interesting perspective is also the investigation of open Floquet systems. When a periodically driven quantum system is coupled weakly to a thermal reservoir, it will eventually reach a quasi-stationary (i.e. time periodic) non-equilibrium steady state. The non-equilibrium nature results from the fact that the transitions induced by the coupling to the bath do not obey detailed balance. Namely a transition $n \rightarrow n'$ between two Floquet states with quasienergies ε_n and $\varepsilon_{n'}$ can be accomplished by changing the bath energy by $\Delta E_B = \varepsilon_n - \varepsilon_{n'} + m\hbar\omega$, where the integer m can take different values. Thus, a particular transition can, for example, occur either by lowering or by raising the bath energy. This becomes apparent in Fermi-golden-rule-type expressions obtained for weak system-bath coupling (Blümel *et al.*, 1991; Hone *et al.*, 2009; Kohler *et al.*, 1997; Lange-meyer and Holthaus, 2014). The resulting asymptotic non-equilibrium steady states can have unconventional properties (e.g. Breuer *et al.*, 2000; Dehghani *et al.*, 2015; Foa Torres *et al.*, 2014; Goldstein *et al.*, 2015; Iadecola *et al.*, 2015; Ketzmerick and Wustmann, 2010; Seetharam *et al.*, 2015; Shirai *et al.*, 2015, 2016; Vorberg *et al.*, 2013, 2015). Unlike thermal states they are not just determined by a few thermodynamic variables like temperature and chemical potential, but depend on the very details of the environment. This makes a theoretical treatment challenging, but opens the door for robust dissipative quantum engineering of driven many-body systems and their properties.

ACKNOWLEDGMENTS

During the last decade, the author had the great pleasure to collaborate and discuss with many colleagues on the subject of periodically driven quantum systems, including Brandon Anderson, Egidijus Anisimovas, Ennio Arimondo, Immanuel Bloch, Alessio Celi, Donatella Ciampini, Sergey Denisov, Omjyoti Dutta, Sebastian Greschner, Peter Hänggi, Masudul Haque, Philipp Hauke, Andreas Hemmerich, Gediminas Juzeliūnas, Roland Ketzmerick, Sigmund Kohler, Achilleas Lazarides, Maciej Lewenstein, Marco di Liberto, Hans Lignier, Tania Monteiro, Cristiane de Morais Smith, Oliver Morsch, Takashi Oka, Christoph Ölschläger, Mirta Rodriguez, Luis Santos, Ulrich Schneider, Alexander Schnell, Klaus Sengstock, Carlo Sias, Juliette Simonet, Ramanjit Sohal, Fernando Sols, Parvis Soltan-Panahi, Shashi Srivastava, Christoph Sträter, Julian Struck, Gayong Sun, Rodolphe Le Targat, Olivier Tieleman, Daniel Vorberg, Malte Weinberg, Christoph Weiss, Christof Weitenberg, Patrick Windpassinger, Waltraut Wustmann, Alessandro Zenesini. Special thanks go to his teacher Martin Holthaus.

REFERENCES

- Abanin, D., W. De Roeck, and W. W. Ho (2015a), arXiv:1510.03405.
- Abanin, D., W. De Roeck, and F. Huveneers (2014), *Ann. Phys.* **372**, 1.
- Abanin, D., W. De Roeck, F. Huveneers, and W. W. Ho (2015b), arXiv:1509.05386.
- Abanin, D. A., W. De Roeck, and F. m. c. Huveneers (2015c), *Phys. Rev. Lett.* **115**, 256803.
- Aidelsburger, M., M. Atala, M. Lohse, J. T. Barreiro, B. Paredes, and I. Bloch (2013), *Phys. Rev. Lett.* **111**, 185301.
- Aidelsburger, M., M. Atala, S. Nascimbène, S. Trotzky, Y.-A. Chen, and I. Bloch (2011), *Phys. Rev. Lett.* **107**, 255301.
- Aidelsburger, M., M. Lohse, C. Schweizer, M. Atala, J. T. Barreiro, S. Nascimbène, N. R. Cooper, I. Bloch, and N. Goldman (2015), *Nat. Phys.* **1**, 162.
- Alberti, A., G. Ferrari, V. V. Ivanov, M. L. Chiofalo, and G. M. Tino (2010), *New J. Phys.* **12**, 065037.
- Alberti, A., V. V. Ivanov, G. M. Tino, and G. Ferrari (2009), *Nature Physics* **5**, 547.
- Anderson, B. M., I. B. Spielman, and G. Juzeliūnas (2013), *Phys. Rev. Lett.* **111**, 125301.
- Anisimovas, E., G. Žlabys, B. M. Anderson, G. Juzeliūnas, and A. Eckardt (2015), *Phys. Rev. B* **91**, 245135.
- Atala, M., M. Aidelsburger, M. Lohse, J. T. Barreiro, B. Paredes, and I. Bloch (2014), *Nat. Phys.* **10**, 588.
- Autler, S. H., and C. H. Townes (1955), *Phys. Rev.* **100**, 703.
- Bakr, W. S., P. M. Preiss, M. E. Tai, R. Ma, J. Simon, and M. Greiner (2011), *Nature* **480**, 500.
- Balents, L. (2010), *Nature* **464**, 199.
- Baur, S. K., M. H. Schleier-Smith, and N. R. Cooper (2014), *Phys. Rev. A* **89**, 051605.
- Bergholtz, E. J., and Z. Liu (2013), *Int. J. Mod. Phys. B* **27** (24), 1330017.

- Bermudez, A., and D. Porras (2015), *New J. Phys.* **17**, 103021.
- Bermudez, A., T. Schätz, and D. Porras (2011), *Phys. Rev. Lett.* **107**, 150501.
- Bilitewski, T., and N. R. Cooper (2015a), *Phys. Rev. A* **91**, 063611.
- Bilitewski, T., and N. R. Cooper (2015b), *Phys. Rev. A* **91**, 033601.
- Blanes, S., F. Casas, J. A. Oteo, and J. Ros (2009), *Physics Reports* **470**, 151.
- Bloch, I., J. Dalibard, and W. Zwerger (2008), *Rev. Mod. Phys.* **80**, 885.
- Blümel, R., A. Buchleitner, R. Graham, L. Sirko, U. Smilansky, and H. Walther (1991), *Phys. Rev. A* **44**, 4521.
- Boll, M., T. A. Hilker, G. Salomon, A. Omran, I. Bloch, and C. Gross (2016), arXiv:1605.05661.
- Breuer, H. P., and M. Holthaus (1989a), *Z. Phys. D* **11**, 1.
- Breuer, H. P., and M. Holthaus (1989b), *Phys. Lett. A* **140**, 507.
- Breuer, H.-P., W. Huber, and F. Petruccione (2000), *Phys. Rev. E* **61**, 4883.
- Bukov, M., L. D'Alessio, and A. Polkovnikov (2015a), *Adv. in Phys.* **64**, 139.
- Bukov, M., S. Gopalakrishnan, M. Knap, and E. Demler (2015b), *Phys. Rev. Lett.* **115**, 205301.
- Canovi, E., M. Kollar, and M. Eckstein (2016), *Phys. Rev. E* **93**, 012130.
- Capogrosso-Sansone, B., N. Prokof'ev, and B. Svistunov (2007), *Phys. Rev. B* **75**, 134302.
- Cardarelli, L., S. Greschner, and L. Santos (2016), arXiv:1604.08829.
- Casas, F., J. A. Oteo, and F. Ros (2000), *J. Phys. A* **34**, 2001.
- Cayssol, J., B. Dóra, F. Simon, and R. Moessner (2013), *Phys. Status Solidi RRL* **7**, 101.
- Chen, Y.-A., S. Nascimbène, M. Aidelsburger, M. Atala, S. Trotzky, and I. Bloch (2011), *Phys. Rev. Lett.* **107**, 210405.
- Choudhury, S., and E. J. Mueller (2014), *Phys. Rev. A* **90**, 013621.
- Choudhury, S., and E. J. Mueller (2015), *Phys. Rev. A* **91**, 023624.
- Chu, S.-I., and D. A. Telnov (2003), *Phys. Rep.* **390**, 1.
- Cohen-Tannoudji, C., J. Dupont-Roc, and G. Grynberg (1998), *Atom-Photon Interactions, Basic Processes and Applications* (Wiley-VCH, Weinheim).
- Creffield, C. E., F. Sols, D. Ciampini, O. Morsch, and E. Arimondo (2010), *Phys. Rev. A* **82**, 035601.
- D'Alessio, L., and M. Rigol (2014), *Phys. Rev. X* **4**, 041048.
- Dalibard, J., F. Gerbier, G. Juzeliūnas, and P. Öhberg (2011), *Rev. Mod. Phys.* **83**, 1523.
- Dehghani, H., T. Oka, and A. Mitra (2015), *Phys. Rev. B* **91**, 155422.
- Denisov, S., L. Morales-Molina, S. Flach, and P. Hänggi (2007), *Phys. Rev. A* **75**, 063424.
- Dreisow, F., M. Heinrich, A. Szameit, S. Döring, S. Nolte, A. Tünnermann, S. Fahr, and F. Lederer (2008), *Opt. Exp.* **16**, 3474.
- Drese, K., and M. Holthaus (1996), *J. Phys.: Condens. Matter* **8**, 1193.
- Drese, K., and M. Holthaus (1997a), *Phys. Rev. Lett.* **78**, 2932.
- Drese, K., and M. Holthaus (1997b), *Chem. Phys.* **217**, 201.
- Drese, K., and M. Holthaus (1999), *Eur. J. Phys. D* **5**, 119.
- Dubček, T., C. J. Kennedy, L. Lu, W. Ketterle, M. Soljačić, and H. Buljan (2014), arXiv:1412.7615.
- Dunlap, D. H., and V. M. Kenkre (1986), *Phys. Rev. B* **34**, 3625.
- Dziarmaga, J. (2010), *Adv. Phys.* **59**, 1063.
- Eckardt, A., and E. Anisimovas (2015), *New J. Phys.* **17**, 093039.
- Eckardt, A., P. Hauke, P. Soltan-Panahi, C. Becker, K. Senstock, and M. Lewenstein (2010), *EPL* **89**, 10010.
- Eckardt, A., and M. Holthaus (2007), *EPL* **80**, 50004.
- Eckardt, A., and M. Holthaus (2008a), *Phys. Rev. Lett.* **101**, 245302.
- Eckardt, A., and M. Holthaus (2008b), *J. Phys.: Conference Series* **99**, 012007.
- Eckardt, A., M. Holthaus, H. Lignier, A. Zenesini, D. Ciampini, O. Morsch, and E. Arimondo (2009), *Phys. Rev. A* **79**, 013611.
- Eckardt, A., C. Weiss, and M. Holthaus (2005), *Phys. Rev. Lett.* **95**, 260404.
- Else, D. V., B. Bauer, and C. Nayak (2016), arXiv:1603.08001.
- Fisher, M. P. A., P. B. Weichman, G. Grinstein, and D. S. Fisher (1989), *Phys. Rev. B* **40**, 546.
- Flach, S., O. Yevtushenko, and Y. Zolotaryuk (2000), *Phys. Rev. Lett.* **84**, 2358.
- Foa Torres, L. E. F., P. M. Perez-Piskunow, C. A. Balseiro, and G. Usaj (2014), *Phys. Rev. Lett.* **113**, 266801.
- Galitski, V., and I. Spielman (2013), *Nature* **494**, 49.
- Gao, F., Z. Gao, X. Shi, Z. Yang, L. Xiao, H. Xu, J. D. Joannopoulos, M. Soljačić, H. Chen, L. Lu, Y. Chong, and B. Zhang (2016), *Nat. Comm.* **7**, 11619.
- Gemelke, N., E. Sarajlic, Y. Bidel, S. Hong, and S. Chu (2005), *Phys. Rev. Lett.* **95**, 170404.
- Genske, M., and A. Rosch (2015), *Phys. Rev. A* **92**, 062108.
- Gesztesy, F., and H. Mitter (1981), *J. Phys. A: Math. Gen.* **14**, L79.
- Goldman, N., and J. Dalibard (2014), *Phys. Rev. X* **4**, 031027.
- Goldman, N., J. Dalibard, M. Aidelsburger, and N. R. Cooper (2015), *Phys. Rev. A* **91**, 033632.
- Goldman, N., G. Juzeliūnas, P. Öhberg, and I. B. Spielman (2014), *Rep. Prog. Phys.* **77**, 126401.
- Goldstein, G., C. Aron, and C. Chamon (2015), *Phys. Rev. B* **92**, 174418.
- Gomez Llorente, J. M., and J. Plata (1992), *Phys. Rev. A* **45**, R6958.
- Gong, J., L. Morales-Molina, and P. Hänggi (2009), *Phys. Rev. Lett.* **103**, 133002.
- Greif, D., T. Uehlinger, G. Jotzu, L. Tarruell, and T. Esslinger (2013), *Science* **340**, 1307.
- Greiner, M., O. Mandel, T. Esslinger, T. W. Hänsch, and I. Bloch (2002), *Nature* **415**, 39.
- Greschner, S., L. Santos, and T. Vekua (2013), *Phys. Rev. A* **87**, 033609.
- Greschner, S., G. Sun, D. Poletti, and L. Santos (2014), *Phys. Rev. Lett.* **113**, 215303.
- Grifoni, M., and P. Hänggi (1998), *Phys. Rep.* **304**, 229.
- Grossmann, F., T. Dittrich, P. Jung, and P. Hänggi (1991), *Phys. Rev. Lett.* **67**, 516.
- Grossmann, F., and P. Hänggi (1992), *EPL* **18**, 571.
- Grozdanov, T. P., and M. J. Raković (1988), *Phys. Rev. A* **38**, 1739.

- Grushin, A. G., A. Gómez-León, and T. Neupert (2014), Phys. Rev. Lett. **112**, 156801.
- Ha, L.-C., L. W. Clark, C. V. Parker, B. M. Anderson, and C. Chin (2015), Phys. Rev. Lett. **114**, 055301.
- Haldane, F. D. M. (1988), Phys. Rev. Lett. **61**, 2015.
- Haller, E., R. Hart, M. J. Mark, J. G. Danzl, L. Reichsöllner, and H.-C. Nägerl (2010), Phys. Rev. Lett. **104**, 200403.
- Haroche, S., C. Cohen-Tannoudji, C. Audoin, and J. P. Schermann (1970), Phys. Rev. Lett. **24**, 861.
- Harper, P. G. (1955), Proceedings of the Physical Society. Section A **68** (10), 874.
- Hart, R. A., P. M. Duarte, T.-L. Yang, X. Liu, T. Paiva, E. Khatami, R. T. Scalettar, N. Trivedi, D. A. Huse, and R. G. Hulet (2015), Nature **519**, 211.
- Hasan, M. Z., and C. L. Kane (2010), Rev. Mod. Phys. **82**, 3045.
- Hauke, P., O. Tieleman, A. Celi, C. Ölschläger, J. Simonet, J. Struck, M. Weinberg, P. Windpassinger, K. Sengstock, M. Lewenstein, and A. Eckardt (2012), Phys. Rev. Lett. **109**, 145301.
- Henneberger, W. C. (1968), Phys. Rev. Lett. **21**, 838.
- Hofstadter, D. R. (1976), Phys. Rev. B **14**, 2239.
- Holthaus, M. (1992), Phys. Rev. Lett. **69**, 351.
- Holthaus, M. (2015), J. Phys. B: At. Mol. Opt. Phys. **49**, 013001.
- Holthaus, M. (2016), J. Phys. B: At. Mol. Opt. Phys. **49**, 013001.
- Holthaus, M., G. H. Ristow, and D. W. Hone (1995), Phys. Rev. Lett. **75**, 3914.
- Hone, D. W., and M. Holthaus (1993), Phys. Rev. B **48**, 15123.
- Hone, D. W., R. Ketzmerick, and W. Kohn (1997), Phys. Rev. A **56**, 4045.
- Hone, D. W., R. Ketzmerick, and W. Kohn (2009), Phys. Rev. E **79**, 051129.
- Hu, W., J. C. Pillay, K. Wu, M. Pasek, P. P. Shum, and Y. D. Chong (2015), Phys. Rev. X **5**, 011012.
- Huber, S. D., and E. Altman (2010), Phys. Rev. B **82**, 184502.
- Iadecola, T., T. Neupert, and C. Chamon (2015), Phys. Rev. B **91**, 235133.
- Itin, A. P., and M. I. Katsnelson (2014), arXiv:1401.0402.
- Ivanov, V. V., A. Alberti, M. Schioppa, G. Ferrari, M. Artoni, M. L. Chiofalo, and G. M. Tino (2008), Phys. Rev. Lett. **100**, 043602.
- Iyer, R., J. S. Aitchison, J. Wan, M. M. Dignam, and C. M. de Sterke (2007), Opt. Exp. **15**, 3212.
- Jaksch, D., C. Bruder, J. I. Cirac, C. W. Gardiner, and P. Zoller (1998), Phys. Rev. Lett. **81**, 3108.
- Jaksch, D., and P. Zoller (2003), New J. Phys. **5**, 56.
- Jiang, L., T. Kitagawa, J. Alicea, A. R. Akhmerov, D. Pekker, G. Refael, J. I. Cirac, E. Demler, M. D. Lukin, and P. Zoller (2011), Phys. Rev. Lett. **106**, 220402.
- Jo, G.-B., J. Guzman, C. K. Thomas, P. Hosur, A. Vishwanath, and D. M. Stamper-Kurn (2012), Phys. Rev. Lett. **108**, 045305.
- Jotzu, G., M. Messer, T. U. Rémi Desbuquois, Martin Lebrat, D. Greif, and T. Esslinger (2014), Nature **515**, 237.
- Karplus, R., and J. M. Luttinger (1954), Phys. Rev. **95**, 1154.
- Keilmann, T., S. Lanzmich, I. McCulloch, and M. Roncaglia (2010), Nat. Comm. **2**, 361.
- Kennedy, C. J., W. C. Burton, W. C. Chung, and W. Ketterle (2015), Nat. Phys. **11**, 859.
- Kennedy, C. J., G. A. Silviloglou, H. Miyake, W. C. Burton, and W. Ketterle (2013), Phys. Rev. Lett. **111**, 225301.
- Ketzmerick, R., and W. Wustmann (2010), Phys. Rev. E **82**, 021114.
- Kierig, E., U. Schnorrberger, A. Schietinger, J. Tomkovic, and M. K. Oberthaler (2008), Phys. Rev. Lett. **100**, 190405.
- Kitagawa, T., E. Berg, M. Rudner, and E. Demler (2010), Phys. Rev. B **82**, 235114.
- Kitagawa, T., M. A. Broome, A. Fedrizzi, M. Rudner, E. Berg, I. Kassal, A. Aspuru-Guzik, E. Demler, and A. G. White (2012), Nat. Comm. **3**, 882.
- Kitagawa, T., T. Oka, A. Brataas, L. Fu, and E. Demler (2011), Phys. Rev. B **84**, 235108.
- Kohler, S., T. Dittrich, P. Hänggi, and T. Dittrich (1997), Phys. Rev. E **55**, 300.
- Kohler, S., J. Lehmann, and P. Hänggi (2005), Phys. Rep. **406**, 379.
- Kolovsky, A. R. (2011), EPL **93**, 20003.
- Kolovsky, A. R., and H. J. Korsch (2010), J. Sib. Fed. Univ. Math. Phys. **3**, 311.
- Ku, M. J. H., A. T. Sommer, L. W. Cheuk, and M. W. Zwierlein (2012), Science **335**, 563.
- Kudo, K., and T. S. Monteiro (2011), Phys. Rev. A **83**, 053627.
- Kuwahara, T., T. Mori, and K. Saito (2016), Annals of Physics **367**, 96.
- Langemeyer, M., and M. Holthaus (2014), Phys. Rev. E **89**, 012101.
- Läuchli, A., and R. Moessner (2015), arXiv:1504.04380.
- Lazarides, A., A. Das, and R. Moessner (2014a), Phys. Rev. E **90**, 012110.
- Lazarides, A., A. Das, and R. Moessner (2014b), Phys. Rev. Lett. **112**, 150401.
- Lazarides, A., A. Das, and R. Moessner (2015), Phys. Rev. Lett. **115**, 030402.
- Lenz, G., R. Parker, M. C. Wanke, and C. M. de Sterke (2003), Opt. Commun..
- Lewenstein, M., A. Sanpera, and V. Ahufinger (2012), *Ultra-cold Atoms in Optical Lattices: Simulating quantum many-body systems* (Oxford University Press, Oxford (UK)).
- Liberto, M. D., C. E. Creffield, G. I. Japaridze, and C. M. Smith (2014), Phys. Rev. A **89**, 013624.
- Lignier, H., C. Sias, D. Ciampini, Y. Singh, A. Zenesini, O. Morsch, and E. Arimondo (2007), Phys. Rev. Lett. **99**, 220403.
- Lim, L., C. M. Smith, and A. Hemmerich (2008), Phys. Rev. Lett. **100**, 130402.
- Lindner, N. H., G. Refael, and V. Galitzki (2012), Nat. Phys. **7**, 490.
- Longhi, S., M. Marangoni, M. Lobino, R. Ramponi, and P. Laporta (2006), Phys. Rev. Lett. **96**, 243901.
- Ma, R., M. E. Tai, P. M. Preiss, W. S. Bakr, J. Simon, and M. Greiner (2011), Phys. Rev. Lett. **107**, 095301.
- Maczewesky, L. J., J. M. Zeuner, S. Nolte, and A. Szameit (2016), arXiv:1605.03877.
- Madison, K. W., M. C. Fischer, R. B. Diener, Q. Niu, and M. G. Raizen (1998), Phys. Rev. Lett. **81**, 5093.
- Maricq, M. M. (1982), Phys. Rev. B **25**, 6622.
- Meinert, F., M. J. Mark, K. Lauber, A. J. Daley, and H.-C. Nägerl (2016), arXiv:1602.02657.
- Mikami, T., S. Kitamura, K. Yasuda, N. Tsuji, T. Oka, and H. Aoki (2016), Phys. Rev. B **93**, 144307.
- Milfeld, K. F., and R. E. Wyatt (1983), Phys. Rev. A **27**, 72.
- Miyake, H., G. A. Silviloglou, J. Kennedy, W. C. Burton, and W. Ketterle (2013), Phys. Rev. Lett. **111**, 185302.

- Moessner, R., and A. P. Ramirez (2006), *Physics Today* **59-2**, 24.
- Möller, G., and N. R. Cooper (2010), *Phys. Rev. A* **82**, 063625.
- Mori, T., T. Kuwahara, and K. Saito (2016), *Phys. Rev. Lett.* **116**, 120401.
- Mukherjee, S., A. Spracklen, M. Valiente, E. Andersson, P. Öhberg, N. Goldman, and R. Thomson (2016), arXiv:1604.05612.
- Oka, T., and H. Aoki (2009), *Phys. Rev. B* **79**, 081406.
- Olf, R., F. Fang, G. E. Martin, A. MacRae, and D. M. Stamper-Kurn (2015), *Nat. Phys.* **11**, 720.
- Orignac, E., and T. Giamarchi (2001), *Phys. Rev. B* **64**, 144515.
- Parameswaran, S. A., R. Roy, and S. L. Sondhi (2013), *C. R. Phys.* **14** (9–10), 816.
- Parker, C. V., L.-C. Ha, and C. Chin (2013), *Nat. Phys.* **9**, 769.
- Peskin, U., and N. Moiseyev (1993), *The Journal of Chemical Physics* **99** (6), 4590.
- Pfeifer, P., and R. D. Levine (1983), *The Journal of Chemical Physics* **79** (11), 5512.
- Platero, G., and R. Aguado (2004), *Phys. Rep.* **395**, 1.
- Poletti, D., and C. Kollath (2011), *Phys. Rev. A* **84**, 013615.
- Poli, N., F.-Y. Wang, M. G. Tarallo, A. Alberti, M. Prevedelli, and G. M. Tino (2011), *Phys. Rev. Lett.* **106**, 038501.
- Polkovnikov, A., K. Sengupta, A. Silva, and M. Vengalattore (2011), *Rev. Mod. Phys.* **83**, 863.
- Ponte, P., Z. Papić, F. m. c. Huvneers, and D. A. Abanin (2015), *Phys. Rev. Lett.* **114**, 140401.
- Qi, X.-L., and S.-C. Zhang (2011), *Rev. Mod. Phys.* **83**, 1057.
- Rahav, S., I. Gilary, and S. Fishman (2003), *Phys. Rev. A* **68**, 013820.
- Rapp, A., X. Deng, and L. Santos (2012), *Phys. Rev. Lett.* **109**, 203005.
- Rechtsman, M. C., J. M. Zeuner, Y. Plotnik, Y. Lumer, D. Podolsky, F. Dreisow, S. Nolte, M. Segev, , and A. Szameit (2013), *Nature* **496**, 196.
- Reichl, M. D., and E. J. Mueller (2014), *Phys. Rev. A* **89**, 063628.
- Rudner, M. S., N. H. Lindner, E. Berg, and M. Levin (2013), *Phys. Rev. X* **3**, 031005.
- Russomanno, A., A. Silva, and G. E. Santoro (2012), *Phys. Rev. Lett.* **109**, 257201.
- Sachdev, S. (2008), *Nat. Phys.* **4**, 173.
- Salger, T., S. Kling, S. Denisov, A. V. Ponomarev, P. Hänggi, and M. Weitz (2013), *Phys. Rev. Lett.* **110**, 135302.
- Salger, T., S. Kling, T. Hecking, C. Geckeler, L. Morales-Molina, and M. Weitz (2009), *Science* **326**, 1241.
- Sambe, H. (1973), *Phys. Rev. A* **7**, 6.
- Seetharam, K. I., C.-E. Bardyn, N. H. Lindner, M. S. Rudner, and G. Refael (2015), *Phys. Rev. X* **5**, 041050.
- Shirai, T., T. Mori, and S. Miyashita (2015), *Phys. Rev. E* **91**, 030101.
- Shirai, T., J. Thingna, T. Mori, S. Denisov, P. Hänggi, and S. Miyashita (2016), *New J. Phys.* **18**, 053008.
- Shirley, J. H. (1965), *Phys. Rev.* **138**, B979.
- Sias, C., H. Lignier, Y. Singh, A. Zenesini, D. Ciampini, O. Morsch, and E. Arimondo (2008), *Phys. Rev. Lett.* **100**, 040404.
- Simon, J., W. S. Bakr, R. Ma, M. E. Tai, P. M. Preiss, and M. Greiner (2011), *Nature* **472**, 307.
- Sørensen, A. S., E. Demler, and M. D. Lukin (2005), *Phys. Rev. Lett.* **94**, 086803.
- Sträter, C., and A. Eckardt (2015), *Phys. Rev. A* (accepted), arXiv:1407.7421.
- Sträter, C., and A. Eckardt (2016), arXiv:1604.00850.
- Sträter, C., S. C. Srivastava, and A. Eckardt (2016), arXiv:1602.08384.
- Struck, J., C. Ölschläger, R. Le Targat, P. Soltan-Panahi, A. Eckardt, M. Lewenstein, P. Windpassinger, and K. Sengstock (2011), *Science* **333**, 996.
- Struck, J., C. Ölschläger, M. Weinberg, P. Hauke, J. Simonet, A. Eckardt, M. Lewenstein, K. Sengstock, and P. Windpassinger (2012), *Phys. Rev. Lett.* **108**, 225304.
- Struck, J., M. Weinberg, C. Ölschläger, P. Windpassinger, J. Simonet, K. Sengstock, R. Höppner, P. Hauke, A. Eckardt, M. Lewenstein, and L. Mathey (2013), *Nat. Phys.* **9**, 738.
- Szameit, A., I. L. Garanovich, M. Heinrich, A. A. Sukhorukov, F. Dreisow, T. Pertsch, S. Nolte, A. Tünnermann, and Y. S. Kivshar (2009), *Nat. Phys.* **5**, 271.
- Szameit, A., I. L. Garanovich, M. Heinrich, A. A. Sukhorukov, F. Dreisow, T. Pertsch, S. Nolte, A. Tünnermann, S. Longhi, and Y. S. Kivshar (2010), *Phys. Rev. Lett.* **104**, 223903.
- Teichmann, N., D. Hinrichs, M. Holthaus, and A. Eckardt (2009), *Phys. Rev. B* **79**, 100503(R).
- Thommen, Q., J. C. Garreau, and V. Zehnlé (2002), *Phys. Rev. A* **65**, 053406.
- Thommen, Q., J. C. Garreau, and V. Zehnlé (2004a), *J. Opt. B: Quantum Semiclass. Opt.* **6**, 301.
- Thommen, Q., J. C. Garreau, and V. Zehnlé (2004b), *Am. J. Phys.* **72**, 1017.
- Thouless, D. J., M. Kohmoto, M. P. Nightingale, and M. den Nijs (1982), *Phys. Rev. Lett.* **49**, 405.
- Trotzky, S., L. Pollet, F. Gerbier, U. Schnorrberger, I. Bloch, N. Prokof'ev, B. Svistunov, and M. Troyer (2009), *Nature Phys.* **6**, 998.
- Račiūnas, M., G. Žlabys, A. Eckardt, and E. Anisimovas (2016), *Phys. Rev. A* **93**, 043618.
- Usaj, G., P. M. Perez-Piskunow, L. E. F. Foa Torres, and C. A. Balseiro (2014), *Phys. Rev. B* **90**, 115423.
- Verdeny, A., A. Mielke, and F. Mintert (2013), *Phys. Rev. Lett.* **111**, 175301.
- Vorberg, D., W. Wustmann, R. Ketzmerick, and A. Eckardt (2013), *Phys. Rev. Lett.* **111**, 240405.
- Vorberg, D., W. Wustmann, H. Schomerus, R. Ketzmerick, and A. Eckardt (2015), *Phys. Rev. E* **92**, 062119.
- Weinberg, M., C. Ölschläger, C. Sträter, S. Prella, A. Eckardt, K. Sengstock, and J. Simonet (2015), *Phys. Rev. A* **92**, 043621.
- Xiao, D., M.-C. Chang, and Q. Niu (2010), *Rev. Mod. Phys.* **82**, 1959.
- Xu, Z.-F., L. You, and M. Ueda (2013), *Phys. Rev. A* **87**, 063634.
- Zak, J. (1993), *Phys. Rev. Lett.* **71**, 2623.
- Zaletel, M. P., S. A. Parameswaran, A. Rüegg, and E. Altman (2014), *Phys. Rev. B* **89**, 155142.
- Zel'dovich, Y. B. (1967), *JETP* **24**, 1006.
- Zenesini, A., H. Lignier, D. Ciampini, O. Morsch, and E. Arimondo (2009), *Phys. Rev. Lett.* **102**, 100403.
- Zhu, M. J., X.-G. Zhao, and Q. Niu (1999), *J. Phys.: Condens. Mat.* **11**, 4527.
- Zwenger, W. (2003), *J. Opt. B: Quantum Semiclass. Opt.* **5**, 9.